de Ronde, C.E.J., Humphris, S.E., Höfig, T.W., and the Expedition 376 Scientists
*Proceedings of the International Ocean Discovery Program* Volume 376
publications.iodp.org

https://doi.org/10.14379/iodp.proc.376.101.2019



# Expedition 376 summary[1]

C.E.J. de Ronde, S.E. Humphris, T.W. Höfig, P.A. Brandl, L. Cai, Y. Cai, F. Caratori Tontini, J.R. Deans, A. Farough, J.W. Jamieson, K.P. Kolandaivelu, A. Kutovaya, J.M. Labonté, A.J. Martin, C. Massiot, J.M. McDermott, I.M. McIntosh, T. Nozaki, V.H. Pellizari, A.G. Reyes, S. Roberts, O. Rouxel, L.E.M. Schlicht, J.H. Seo, S.M. Straub, K. Strehlow, K. Takai, D. Tanner, F.J. Tepley III, and C. Zhang[2]

Keywords: International Ocean Discovery Program, IODP, *JOIDES Resolution*, Expedition 376, Brothers Arc Flux, Brothers volcano, Site U1527, Site U1528, Site U1529, Site U1530, Site U1531, Kermadec arc, submarine arc volcano, hydrothermal systems, volcaniclastics, dacite lava, hydrothermal alteration, borehole fluids, hypersaline brine, fluid inclusions, acidic fluids, alteration mineral assemblages, Upper Cone, Lower Cone, NW Caldera

Contents



## Abstract

Volcanic arcs are the surface expression of magmatic systems that result from subduction of mostly oceanic lithosphere at convergent plate boundaries. Arcs with a submarine component include intraoceanic arcs and island arcs that span almost 22,000 km on Earth's surface, and the vast majority of them are located in the Pacific region. Hydrothermal systems hosted by submarine arc volcanoes commonly contain a large component of magmatic fluid. This magmatic-hydrothermal signature, coupled with the shallow water depths of arc volcanoes and their high volatile contents, strongly influences the chemistry of the fluids and resulting mineralization and likely has important consequences for the biota associated with these systems. The high metal content and very acidic fluids in these hydrothermal systems are thought to be important analogs to numerous porphyry copper and epithermal gold deposits mined today on land.

During International Ocean Discovery Program (IODP) Expedition 376 (5 May–5 July 2018), a series of five sites was drilled on Brothers volcano in the Kermadec arc. The expedition was designed to provide the missing link (i.e., the third dimension) in our understanding of hydrothermal activity and mineral deposit formation at submarine arc volcanoes and the relationship between the discharge of magmatic fluids and the deep biosphere. Brothers volcano hosts two active and distinct hydrothermal systems: one is seawater influenced and the other is affected by magmatic fluids (largely gases). In total, 222.4 m of volcaniclastics and lavas were recovered from the five sites drilled, which include Sites U1527 and U1530 in the Northwest (NW) Caldera seawater-influenced hydrothermal field; Sites U1528 and U1531 in the magmatic fluid-influenced hydrothermal fields of the Upper and Lower Cones, respectively; and Site U1529, located within an area of low crustal magnetization that marks the West (W) Caldera upflow zone on the caldera floor. Downhole logging and borehole fluid sampling were completed at two sites, and two tests of a prototype turbine-driven coring system (designed by the Center for Deep Earth Exploration [CDEX] at Japan Agency for Marine-Earth Science and Technology [JAMSTEC]) for drilling and coring hard rocks were conducted.

Core recovered from all five sites consists of dacitic volcaniclastics and lava flows with only limited chemical variability relative to the overall range in composition of dacites in the Kermadec arc. Pervasive alteration with complex and variable mineral assemblages attest to a highly dynamic hydrothermal system. The upper parts of several drill holes at the NW Caldera hydrothermal field are characterized by secondary mineral assemblages of goethite + opal + zeolites that result from low-temperature (<150°C) reaction of rock with seawater. At depth, NW Caldera Site U1527 exhibits a higher temperature (~250°C) secondary mineral assemblage dominated by chlorite + quartz + illite + pyrite. An older mineral assemblage dominated by diaspore + quartz + pyrophyllite + rutile at the bottom of Hole U1530A is indicative of acidic fluids with temperatures of ~230°–320°C. In contrast, the alteration assemblage at Site U1528 on the Upper Cone is dominated by illite + natroalunite + pyrophyllite + quartz + opal + pyrite, which attests to high-temperature reaction of rocks with acid-sulfate fluids derived from degassed magmatic volatiles and the disproportionation of magmatic $SO_2$. These intensely altered rocks exhibit extreme depletion of major cation oxides, such as MgO, $K_2O$, CaO, MnO, and $Na_2O$. Furthermore, very acidic (as low as pH 1.8), relatively hot (≤236°C) fluids collected at 160, 279, and 313 meters below seafloor in Hole

[1] de Ronde, C.E.J., Humphris, S.E., Höfig, T.W., Brandl, P.A., Cai, L., Cai, Y., Caratori Tontini, F., Deans, J.R., Farough, A., Jamieson, J.W., Kolandaivelu, K.P., Kutovaya, A., Labonté, J.M., Martin, A.J., Massiot, C., McDermott, J.M., McIntosh, I.M., Nozaki, T., Pellizari, V.H., Reyes, A.G., Roberts, S., Rouxel, O., Schlicht, L.E.M., Seo, J.H., Straub, S.M., Strehlow, K., Takai, K., Tanner, D., Tepley, F.J., III, and Zhang, C., 2019. Expedition 376 summary. *In* de Ronde, C.E.J., Humphris, S.E., Höfig, T.W., and the Expedition 376 Scientists, *Brothers Arc Flux*. Proceedings of the International Ocean Discovery Program, 376: College Station, TX (International Ocean Discovery Program). https://doi.org/10.14379/iodp.proc.376.101.2019

[2] **Expedition 376 Scientists' affiliations.**

MS 376-101: Published 5 July 2019

U1528D have chemical compositions indicative of magmatic gas input. In addition, preliminary fluid inclusion data provide evidence for involvement of two distinct fluids: phase-separated (modified) seawater and a ~360°C hypersaline brine, which alters the volcanic rock and potentially transports metals in the system.

The material and data recovered during Expedition 376 provide new stratigraphic, lithologic, and geochemical constraints on the development and evolution of Brothers volcano and its hydrothermal systems. Insights into the consequences of the different types of fluid–rock reactions for the microbiological ecosystem elucidated by drilling at Brothers volcano await shore-based studies.

## Introduction

Magmatic systems that derive from subduction of mainly oceanic lithosphere at convergent plate boundaries become manifest in volcanic arcs at the surface. Those arcs that contain a submarine component include intraoceanic arcs and island arcs, which span almost 22,000 km on Earth's surface, the vast majority of which are located in the Pacific region (de Ronde et al., 2003). It is estimated that all intraoceanic arcs combined may contribute hydrothermal emissions equal to ~10% of that from mid-ocean ridges (MORs) (Baker et al., 2008).

Hydrothermal activity associated with these submarine arc volcanoes is commonly dominated by discharge of magmatic volatiles in contrast to MOR systems that are governed by seawater circulation through basaltic oceanic crust. Submarine arc magmatic-hydrothermal systems are driven by crystallization of magmas produced by mantle melting fluxed by volatiles released from the subducting slab. These magmas are enriched by an order of magnitude in volatiles compared with MOR basalts (e.g., Wallace, 2005; Plank et al., 2013). Degassing of these arc magmas gives rise to extraordinary phenomena, such as the discharge of liquid $CO_2$ (Lupton et al., 2006) and the formation of liquid "lakes" of sulfur on the seafloor (de Ronde et al., 2015). Although intraoceanic arcs are some of the most hostile environments for life because of the exceptionally high concentrations of toxic metals and metalloids in very acidic, gas-rich, high-temperature fluids, diverse animal and microbial communities are commonly observed (e.g., Clark and O'Shea, 2001; Takai et al., 2009).

The Kermadec segment of the Kermadec-Tonga intraoceanic arc (Figure **F1**) is host to ~32 large volcanoes, 80% of which are hydrothermally active, making it the most active arc in the world. The magmatic-hydrothermal signatures, including high concentrations of sulfur and carbon species gases and high iron contents, coupled with the shallow depths of venting (~1800–120 meters below sea level [mbsl]) of these volcanoes, heavily influence the chemistry of the discharging fluids and the minerals that precipitate from these fluids and have important consequences for the biota associated with these systems. Given the high metal contents and very acidic fluids, these hydrothermal systems are also considered to serve as important submarine analogs to many of the porphyry copper and epithermal gold deposits exploited on land today.

Brothers volcano on the Kermadec arc is such a system and has been the focus of a continuing series of studies. An International Ocean Discovery Program (IODP) workshop (Lisbon, November 2012; **http://www.ecord.org/science/magellanplus**) identified Brothers volcano as the top candidate worldwide for arc volcano drilling. Hence, Expedition 376 was designed to provide the missing link (i.e., the third dimension) in our understanding of mineral deposit formation along arcs, the subseafloor architecture of these volcanoes and their related permeability, and the relationship between the discharge of magmatic fluids and the deep biosphere.

Figure F1. Bathymetric map of the Kermadec arc, trench, and major tectonic elements. Brothers volcano is located on the active volcanic front in the southern half of the arc. From de Ronde et al. (2012).

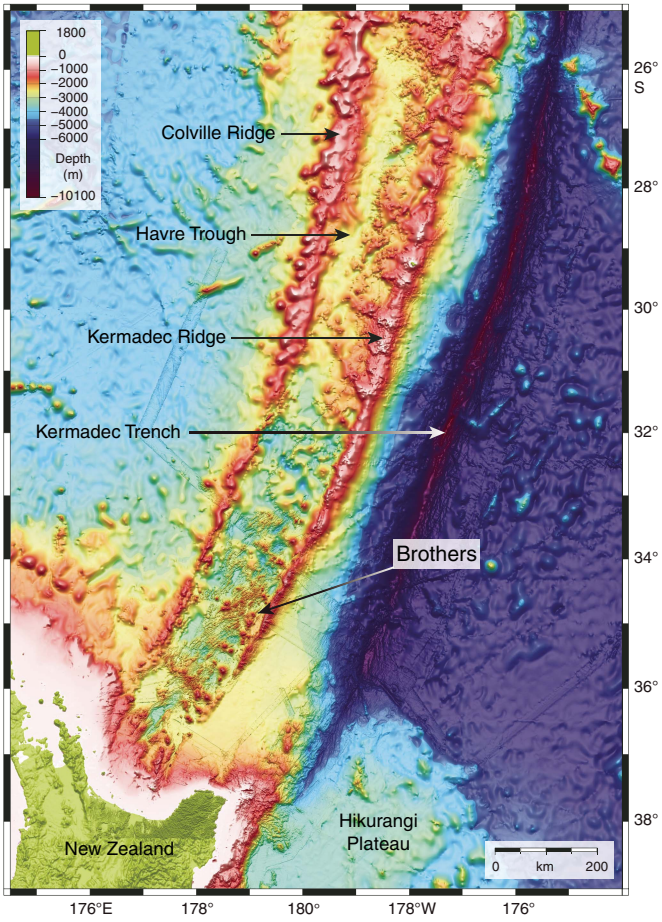


## Geological setting

The Kermadec-Tonga arc northeast of New Zealand (Figure **F1**) is one of the longest contiguous intraoceanic arcs in the world. More than 60 volcanoes of varying sizes occur along the arc—the vast majority of which are submarine—with more than half occurring in the Kermadec sector (de Ronde et al., 2003, 2007). Volcanic rocks along the Kermadec arc range in composition from basalt to rhyodacite. Trace element and isotopic data indicate significant magma source heterogeneity both along and across the arc as a result of variable subduction of continent-derived sediments, pelagic sediments, and oceanic crust and/or interaction with continental crust (e.g., Gamble and Wright, 1995; Gamble et al., 1996; Haase et al., 2002; Timm et al., 2012, 2013, 2014).

Brothers volcano (Figure **F2**) is one of three caldera volcanoes included in 13 major volcanic edifices that form the active Kermadec volcanic arc front between 37°S and 34°50′S (Wright, 1997; Wright and Gamble, 1999). Brothers volcano is part of a ~35 km long and 15 km wide predominantly silicic volcanic complex that is dissected by basement fractures and associated dike-controlled ridges that are 1–1.5 km wide and rise 400–500 m above the seafloor. These structures strike predominantly 55° to 65°, although a

Figure F2. Detailed bathymetry of Brothers volcano and surrounding area. Dashed lines = structural ridges. NF = North fault, SF = South fault, NRZ = North rift zone, UC = Upper Cone, LC = Lower Cone, UCald = Upper Caldera, NWC = NW Caldera, WC = W Caldera, SEC = SE Caldera, RTR = regional tectonic ridge. A–B (coincident with Seismic Line Bro-3) and C–D are endpoints for the bathymetric cross sections shown in the top panels. Contour interval = 200 m. Modified from Embley et al. (2012).

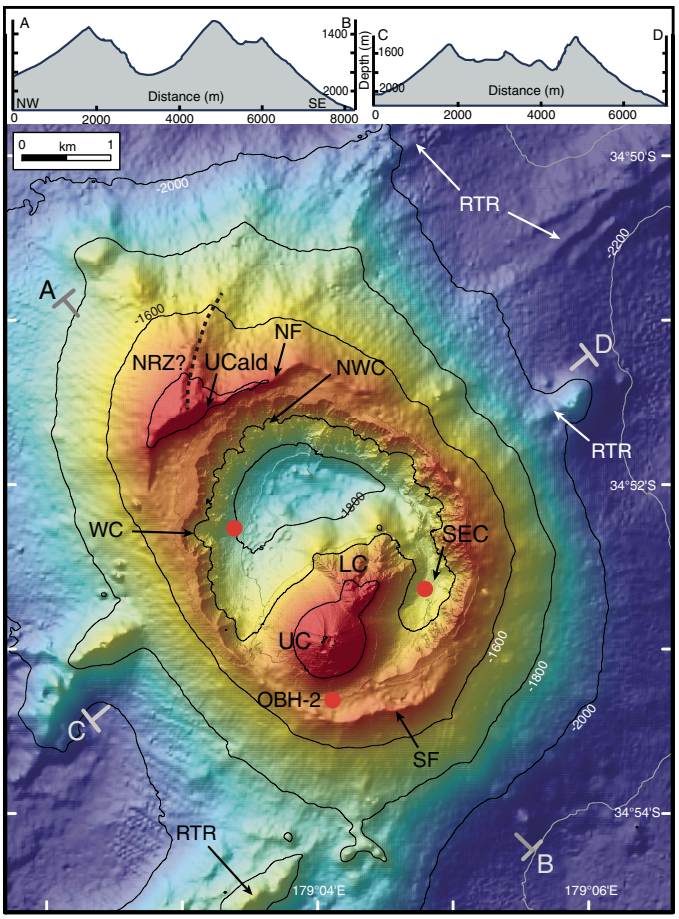


conjugate set of faults is observed subparallel to the elongated Brothers volcano edifice and caldera (Figure F2). These orientations are consistent with Havre Trough rifting (e.g., Wright et al., 1996; Deltiel et al., 2002; Ruellen et al., 2003) and indicate first-order extensional tectonic control on Brothers volcano. The base of Brothers volcano rises from a water depth of ~2200 m to a continuous caldera rim at 1540 m, although locally the northwestern rim (or Upper Caldera wall) shoals to 1320 m. The caldera floor has a basal diameter of 3–3.5 km, reaches a water depth of 1850 m, and is surrounded by 290–530 m high walls. An elongated northeast–southwest postcollapse cone (1.5–2 km wide × 350 m high), the Upper Cone, occurs within the caldera, and a satellite cone (Lower Cone) appears on its northeastern flank (Figure F3A, F3B). The Upper Cone in part coalesces with the southern caldera wall and shoals to 1220 mbsl (de Ronde et al., 2005).

Brothers volcano represents a window into the complicated hydrothermal systems found at submarine arc volcanoes, which display a range of geological and structural settings and vent fluid chemistry, as well as animals and microbes as yet undiscovered at any other site on the seafloor. Six hydrothermal fields have been identified in or on the walls of the caldera at Brothers volcano (Figures F2, F4). Five of these fields are presently active (the Upper Caldera, Northwest [NW] Caldera, West [W] Caldera, Upper Cone, and Lower Cone sites), whereas the Southeast (SE) Caldera site is currently inactive, or at least it does not contribute to vent plumes measured above the seafloor (Baker et al., 2012). Extensive autonomous underwater vehicle (AUV) mapping of the caldera (de Ronde et al., 2012; Embley et al., 2012) has shown that these hydrothermal fields, with the exception of the Lower Cone site, are closely correlated to areas of low crustal magnetization that are consistent with zones of hydrothermal upflow (Figure F5) (Caratori Tontini et al., 2012a, 2012b; Gruen et al., 2012).

The five active fields exhibit two different types of hydrothermal activity. Type I hydrothermal systems are characterized by high-temperature (≤320°C) venting of relatively gas-poor, moderately acidic fluids at the W, NW, and Upper Caldera sites, where Cu-Au–rich sulfide chimneys are common. Type II hydrothermal fields are characterized by lower temperature (≤120°C) venting of gassy, very low pH (to 1.9) fluids at the summits of the Upper and Lower Cone sites, where native sulfur chimneys and extensive Fe oxyhydroxide crusts occur (de Ronde et al., 2005, 2011). Time-series studies of hydrothermal plumes above the four most active sites (i.e., Upper Caldera, NW Caldera, and the Upper and Lower Cone sites) show that the cone sites expelled fluids of widely differing compositions between 1999 and 2018, with large variations in dissolved $H_2S$, particulate Cu, dissolved Fe, and Fe/Mn values (Humphris et al., 2018). By contrast, the composition of chronic plumes above the NW Caldera site (the Upper Caldera site was discovered only in 2017), although chemically distinct from the other hydrothermal vent sites, has not changed over the same interval (de Ronde et al., 2005; Humphris et al., 2018).

In 2005, Neptune Minerals Inc. drilled a number of shallow holes (to 14.8 meters below seafloor [mbsf]) at Brothers volcano. Sixteen holes were drilled on the slopes of the NW Caldera wall, and a single hole was drilled inside the crater atop the Upper Cone. The uppermost material of many of these holes consisted of dark brown ooze locally containing glass sand and grit. This material was commonly underlain by an ~1 m thick zone that contained pieces of sulfide chimney, glass grit, Fe-Si-Mn oxyhydroxides, and mixtures thereof. Typically underlying this zone were variably hydrothermally altered volcanic rocks ranging from volcanic silt and sand to volcanic glass, gravel, breccia, and more massive volcanic rock (dacite). Alteration colors ranged from pale gray to pale green, and stockwork veins locally cut the rocks. The one core drilled inside the pit crater atop the Upper Cone intersected volcanic breccia, gravels, and rocks together with native sulfur to 10 mbsf.

Microbial community development patterns associated with the two types of hydrothermal activity at Brothers volcano have been explored using limited (four) samples collected from the seafloor (Stott et al., 2008; Takai et al., 2009). Microbial community compositions obtained from chimneys at the NW Caldera site are characterized by an abundance of slightly thermophilic and hyperthermophilic chemolithoautotrophs (Takai et al., 2009), which are observed in typical high-temperature hydrothermal vent environments of MORs and back-arc basin systems (Nakamura and Takai, 2014). By contrast, microbial communities from the Lower Cone exhibit a diversity of bacterial lineages, with potential psychrophilic and thermophilic sulfur- and iron-oxidizing chemolithotrophs (Stott et al., 2008) like those found in the magmatic volatile–rich hydrothermal environments of submarine arc volcanoes (Nakamura and Takai, 2014). These intrafield differences in microbial community composition and function are thought to be associated

Figure F3. A. AUV tracks from the 2007 *ABE* dives (colored tracks) and the 2011 *Sentry* dive (white tracks). Figure from Baker et al. (2012). B. Results of the high-resolution (~2 m) mapping of the caldera walls and cones from the *ABE* survey overlain on EM300 bathymetric survey (~25 m resolution) data for the caldera floor, Upper Caldera walls in the northwest, and the outside flanks of the volcano. From Merle et al. (2007) and reproduced with some modification in Embley et al. (2012).

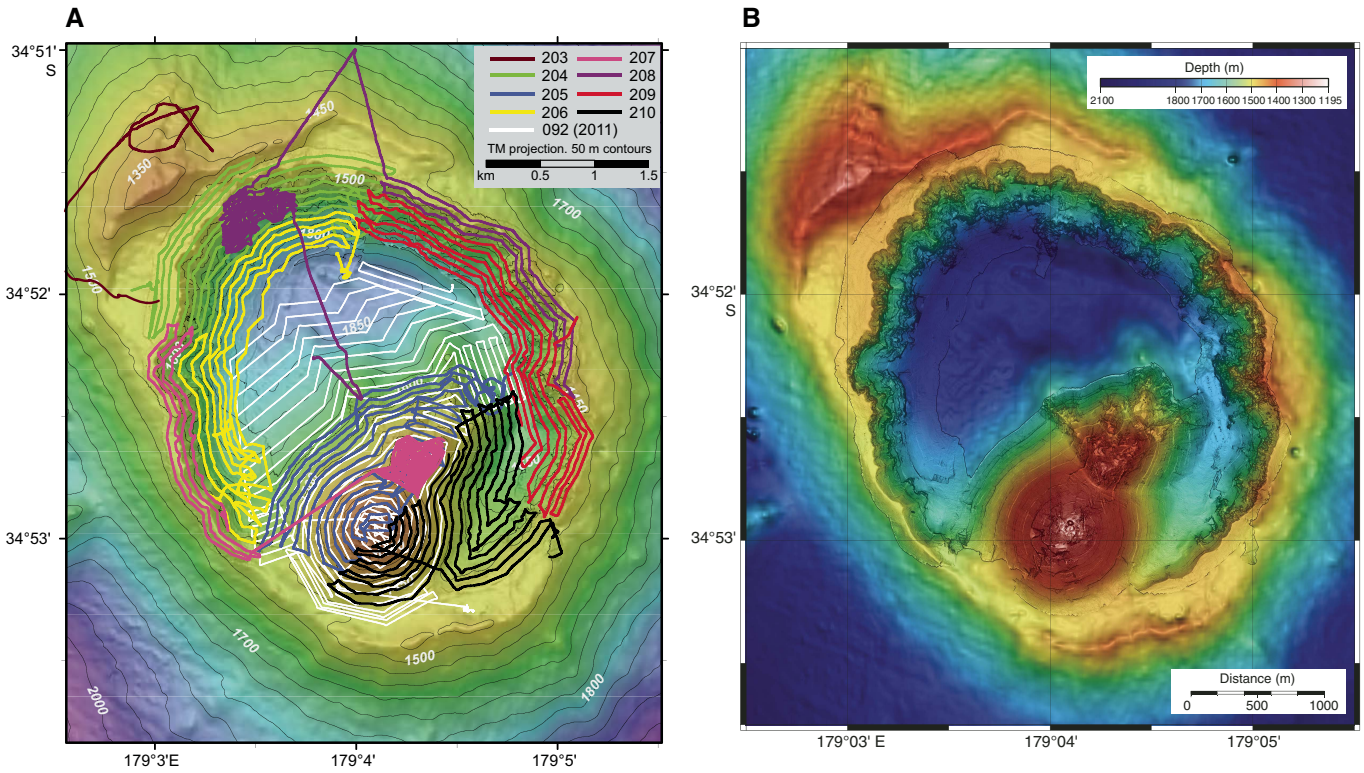


with the different hydrothermal fluid compositions in the two types of hydrothermal systems. In particular, the highly variable volatile species concentrations induced by phase separation, the variable mixing ratios of hydrothermal and seawater inputs, and the concomitant precipitation of mineral phases are considered crucial factors in the control of chemosynthetic microbial community development (Takai and Nakamura, 2011; Nakamura and Takai, 2014). The common occurrence of two distinct hydrothermal microbial ecosystems within a single caldera, showing a clear niche segregation in response to both physical and chemical differences in the hydrothermal fluids, is currently globally unique (Flores et al., 2012; Nakamura and Takai, 2014).

Modeling of the subseafloor hydrology at Brothers volcano has suggested that subseafloor phase separation, inferred from measured temperatures and calculated end-member vent fluid chemical and isotopic compositions, can be achieved only by the primary input of saline magmatic fluids at depth (de Ronde et al., 2011; Gruen et al., 2012, 2014). In addition, the vent systems appear to evolve over short time periods. Expulsion of magmatic heat and volatiles occurs within the first few hundred years of magma emplacement in the form of low-salinity, vapor-rich fluid, and magmatically derived salt is temporarily trapped in the crust. This retained salt is then periodically expelled from the system by later convection of low- to high-temperature hydrothermal fluid of seawater origin (Gruen et al., 2014). This model has important implications for the distribution of metals in the hydrothermal mineralization. Sulfide-complexed metals (e.g., Au) will preferentially ascend during the early vapor-dominated fluid discharge, whereas chloride-complexed metals (e.g., Cu, Pb, and Zn) will be retained in the dense magmatic brine, thus potentially forming layers of metal sulfides with distinct zonation at depth (Gruen et al., 2014).

Figure F4. Distribution of plume tracers in (A–D) 2007 using the *ABE* survey and in (E, F) 2011 using the *Sentry* survey overlain on bathymetry from Figure F3B. Light blue shaded area in some panels marks area of Dive 205 survey (see Figure F3A) where no Δ nephelometric turbidity units (ΔNTU) or dE/dt data were recorded. A. Δθ (°C) anomalies. B. ΔNTU anomalies. C. dE/dt (mV/s) anomalies. D. Fluid discharge types inferred from ΔNTU/Δθ values. E. ΔNTU anomalies. F. dE/dt (mV/s) anomalies. Plots from Baker et al. (2012).

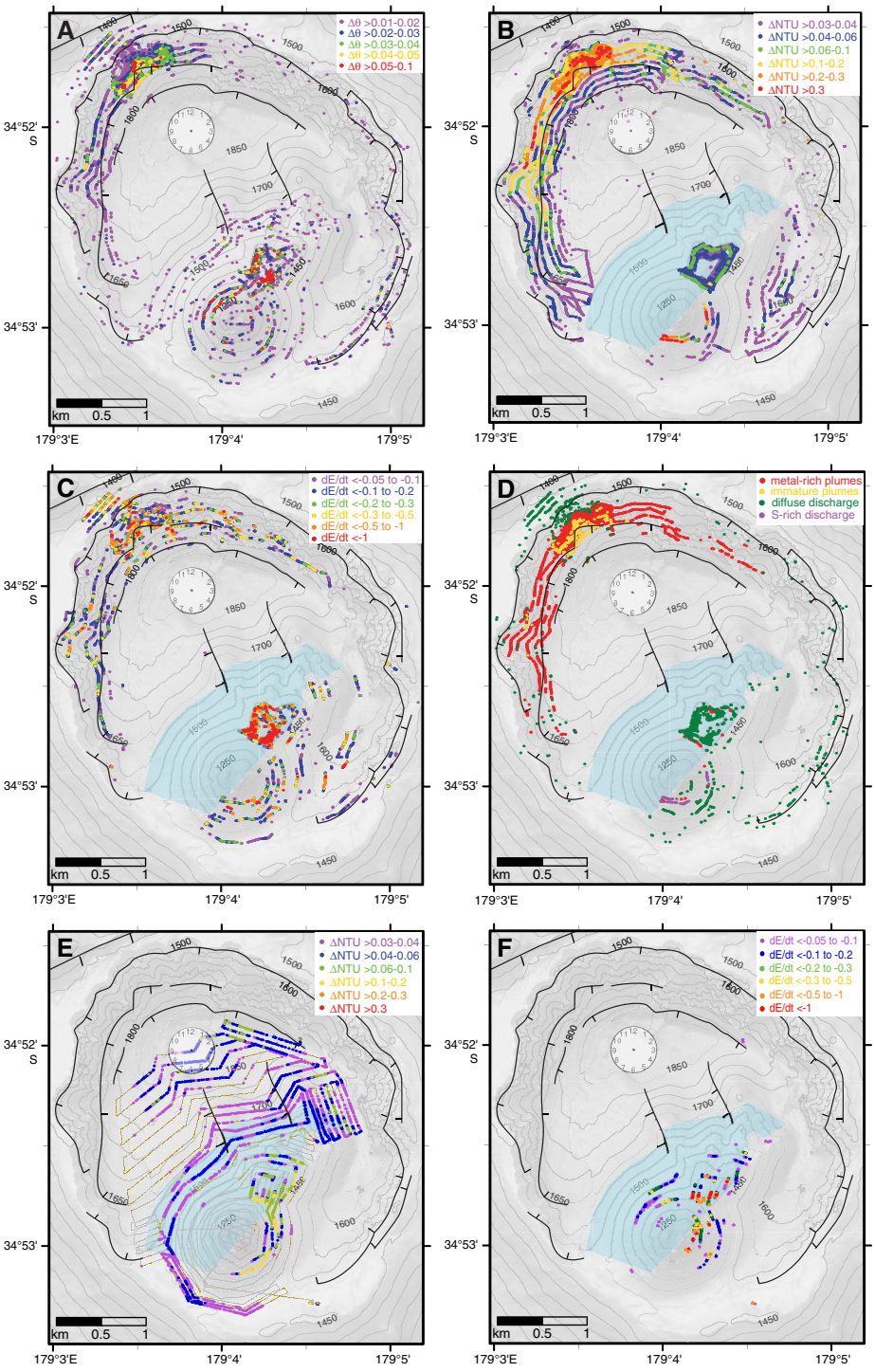

Figure F5. Apparent magnetization map of Brothers volcano showing reduced crustal magnetization over four areas that include five hydrothermal vent sites. A = Upper Caldera and NW Caldera, B = Upper Cone, C = SE Caldera, D = W Caldera. Outlined areas have either very low (<2.5 A/m; Zones A and D) or moderate (<3.5 A/m; Zones B and C) magnetization, which is in general agreement with the location of the various vent fields. The Lower Cone hydrothermal vent site is situated immediately northeast of Zone B and does not have an associated reduced crustal magnetization signature. Zone C is largely an extinct vent site. Structural lineaments (white lines) and ring faults (white lines with hash marks) are shown for reference. Figure from Caratori Tontini et al. (2012a).

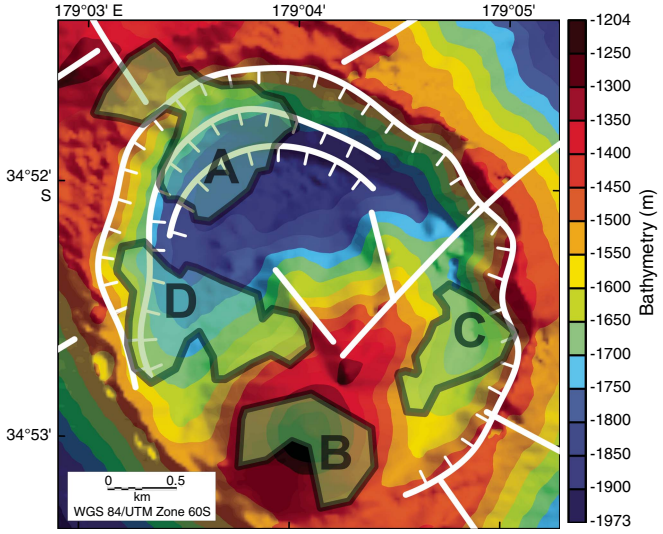


## Scientific objectives

The following four primary scientific objectives were outlined in the Expedition 376 *Scientific Prospectus* (de Ronde et al., 2017):

- Characterize the subvolcano, magma chamber–derived volatile phase to test model-based predictions that this is either a single-phase gas or two-phase brine-vapor;
- Determine the subseafloor distribution of base and precious metals and metalloids and the reactions that have taken place along pathways to the seafloor;
- Quantify the mechanisms and extent of fluid–rock interaction and consequences for mass transfer of metals and metalloids into the ocean and the role of magmatically derived carbon and sulfur species in mediating these fluxes; and
- Assess the diversity, extent, and metabolic pathways of microbial life in an extreme, metal-toxic, acidic volcanic environment.

The drill sites represent discharge zones of geochemically distinct fluids that are variably affected by magmatic volatile input, allowing us to directly address the consequences of magma degassing on metal transport to the seafloor and its effect on the functioning of microbial communities.

To meet these objectives, a strategy involving two independent drilling efforts was developed to recover cores from both shallow (<200 mbsf) and deep (~200–800 mbsf) intervals. Cores with good recovery are required from the shallowest intervals (tens of meters depth) to examine aspects of hydrogeology, permeability, fluid flow, and seawater entrainment and their effects on microbial community development and habitability. We will acquire these cores by deploying the MeBo seafloor drill rig (Freudenthal and Wefer, 2007) from R/V *Sonne* at a time yet to be planned (Bach, Haase, Wefer, and de Ronde, co-Principal Investigators). This scheduled shallow drilling allowed Expedition 376 to bypass coring in the shallowest parts of the holes when necessary and strategically prepare the holes for casing installations required for deep coring. The operational plan for Expedition 376 was to drill, core, and log three sites, one on the northwest rim of the caldera, one on the western side of the caldera floor, and one atop the Upper Cone, to provide access to critical zones dominated by magma degassing and high-temperature hydrothermal circulation over depth ranges considered crucial in the development of multiphase mineralizing systems.

## Site summaries

### Site U1527

#### Background and objectives

Site U1527 (proposed Site NWC-1A) is located on the rim of the northwest caldera wall of Brothers volcano at a water depth of 1464 m (Figure **F6**). Drilling targeted what was thought to be either the margin of an older modified-seawater hydrothermal upflow zone or a recharge zone to the currently active discharge areas several hundred meters away from either side of the drill site. A key objective of Expedition 376 was to quantify the mechanisms and extent of fluid–rock interaction and the consequences for mass transfer of metals into the ocean in both seawater-dominated and magmatic fluid–dominated hydrothermal systems within the caldera of Brothers volcano. Hence, the main objective of Site U1527 was to drill through the margin of the inferred upflow zone of a modified-seawater system.

#### Operations

We conducted operations in three holes at Site U1527 (Table **T1**). Hole U1527A is located at 34°51.6528′S, 179°3.2397′E at a water depth of 1464.2 m. We used the rotary core barrel (RCB) system in this hole to core from the seafloor to 101.4 mbsf. Recovery was poor (1.27 m; 1.3%). The downhole conditions encountered in Hole U1527A determined the preparations for running a reentry system. In Hole U1527B, located at 34°51.6519′S, 179°3.2526′E at a water depth of 1464.2 m, 10¾ inch (~27.3 cm) casing was drilled in to 95.5 mbsf, and final penetration of the drilling assembly was 105.5 mbsf. Upon release from the casing, the reentry system hung up on the underreamer arms, which failed to retract, and the entire assembly was recovered to the surface.

Hole U1527C is located at 34°51.6625′S, 179°3.2534′E at a water depth of 1464.1 m. After installing 95.5 m of casing, we continuously cored with the RCB system from 99.9 to 238.0 mbsf and recovered 25.9 m (19%) of material. We had extremely poor to no recovery in unconsolidated volcanic deposits until a formation change at 187 mbsf, where average recovery increased to 49% for the rest of coring in cemented volcaniclastic rocks. Unstable hole conditions forced abandonment of Hole U1527C and, once again, the reentry system was unintentionally retrieved because of clogging of the hydraulic release tool (HRT) and upper casing sub. In total, 249.6 h, or 10.4 days, were spent at Site U1527.

#### Principal results

Igneous rocks cored at Site U1527 were divided into two units (Figure **F7**). Igneous Unit 1 was recovered in Holes U1527A (29.10–67.81 mbsf) and U1527C (108.40–176.16 mbsf). This unit consists of plagioclase-clinopyroxene-phyric and Fe-Ti oxide–bearing black dacite lava with glassy trachytic groundmass and spatially associated fresh scoria and pumice lapilli.

Igneous Unit 2 was recovered in Hole U1527C (185.20–234.38 mbsf). The contact between Igneous Units 1 and 2 was not recovered. Igneous Unit 2 consists of progressively hydrothermally altered lapilli-tuffs, tuff-breccias, and lapillistone and is divided into four subunits (2a–2d) based on changes in modal composition of clasts, matrix-to-clast ratio, and color. Subunit 2a (185.20–185.44 mbsf) is lapilli-tuffs consisting of fresh dacitic clasts surrounded by a brown, fine-grained matrix that probably represents altered tuff. Subunit 2b (185.44–220.98 mbsf) is composed of matrix-supported monomict and polymict lapilli-tuffs, lapillistones, and tuff-breccias.

Figure F6. Detailed bathymetry (contour interval is 200 m) of Brothers volcano and surrounding area showing the location of sites drilled during Expedition 376: U1527, U1528, U1529, U1530, and U1531 (modified from Embley et al., 2012).

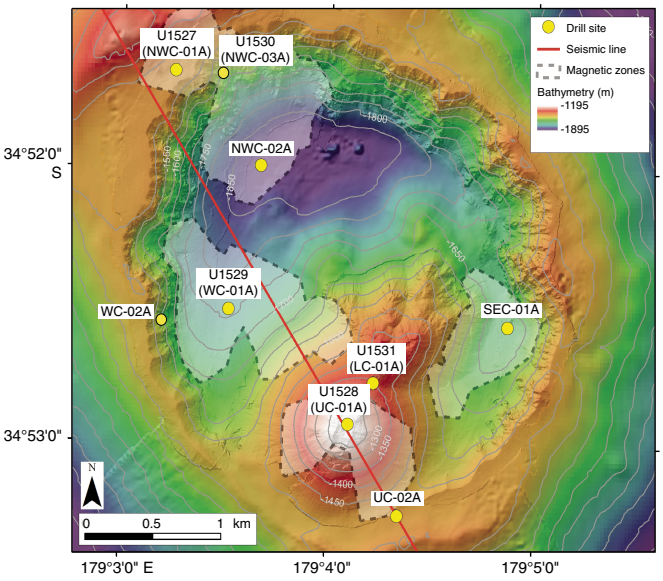


Subunit 2c (220.98–226.49 mbsf) is made up of clast-supported polymict lapillistones, and Subunit 2d (228.40–234.38 mbsf) is composed of both altered matrix-supported and clast-supported tuff-breccias and lapilli-tuffs.

Igneous Unit 2 rocks contain various clasts of volcanic origin:

- Unaltered to slightly altered dacite in Subunit 2a,
- Volumetrically significant greenish gray altered volcanic clasts in Subunits 2b–2d,
- Fine-grained, dark green altered clasts in Subunit 2b, and
- Various types of rare dark gray volcanic clasts in Subunits 2b–2d.

The matrix of the volcaniclastic rocks and the groundmass within volcanic clasts in Igneous Unit 2 appear very similar to the trachytic groundmass of the dacite lava of Igneous Unit 1, but they are increasingly replaced by secondary chlorite, clays, and quartz with depth. All clasts contain varying amounts of plagioclase, clinopyroxene, and Fe-Ti oxides, strongly resembling the primary phenocryst assemblage of the dacite lava of Unit 1. Although the degree of alteration increases downhole, as indicated by the increasing degree of silicification, plagioclase crystals are only slightly altered, whereas clinopyroxene is altered significantly or disappears, and Fe-Ti oxides alter to sulfides.

Three distinct types of alteration are observed in core material recovered from Site U1527 (Figure F8). Alteration Type I (0–185.44 mbsf) occurs in intervals of fresh to slightly altered volcanic rocks and is characterized by low-temperature alteration mineral assemblages (Figure F9). This alteration type is divided into two distinct subtypes. Subtype Ia (0–185.20 mbsf) occurs within unaltered to slightly altered vesicular dacite lava and is characterized by the presence of zeolite in vesicles and the occurrence of palagonite, Fe oxyhydroxide, and trace pyrite partly replacing volcanic glass. Subtype Ib (185.20–185.44 mbsf) solely pertains to the volcaniclastic rocks of Igneous Subunit 2a, which are slightly to moderately altered. The clasts exhibit only trace alteration and retain primary plagioclase

Table T1. Hole summary, Expedition 376. NA = not applicable. * = Includes return at end of expedition for downhole measurements. **Download table in CSV format.**

| Hole | Latitude | Longitude | Water depth (mbsl) | Cores (*N*) | Interval cored (m) | Core recovered (m) | Recovery (%) | Drilled interval (m) | Total penetration (m) | Time on hole (h) | Time at site (days) |
|---|---|---|---|---|---|---|---|---|---|---|---|
| U1527A | 34°51.6528′S | 179°03.2397′E | 1464.23 | 15 | 101.4 | 1.27 | 1.25 | 0 | 101.4 | 51.3 | |
| U1527B | 34°51.6519′S | 179°03.2526′E | 1464.19 | NA | NA | NA | NA | 105.5 | 105.5 | 76.3 | |
| U1527C | 34°51.6625′S | 179°03.2534′E | 1464.12 | 19 | 138.1 | 25.9 | 18.75 | 99.9 | 238.0 | 122.0 | |
| | | | Site U1527 totals: | 34 | 239.5 | 27.17 | 11.34 | 205.4 | 444.9 | | 10.4 |
| U1528A | 34°52.9177′S | 179°04.1070′E | 1228.36 | 15 | 84.4 | 17.09 | 20.25 | 0 | 84.4 | 50.3 | |
| U1528B | 34°52.9222′S | 179°04.1077′E | 1240.30 | NA | NA | NA | NA | 25.6 | 25.6 | 79.3 | |
| U1528C | 34°52.9215′S | 179°04.1128′E | 1229.01 | 7 | 31.5 | 3.63 | 11.52 | 22 | 53.5 | 47.8* | |
| U1528D | 34°52.9219′S | 179°04.1164′E | 1228.04 | 62 | 298.0 | 87.23 | 29.27 | 61.3 | 359.3 | 391.5 | |
| | | | Site U1528 totals: | 84 | 413.9 | 107.95 | 26.08 | 108.9 | 522.8 | | 23.7 |
| U1529A | 34°52.5161′S | 179°03.5139′E | 1734.99 | 1 | 12.0 | 1.86 | 15.5 | 0 | 12.0 | 15.0 | |
| U1529B | 34°52.5217′S | 179°03.5207′E | 1732.99 | 4 | 34.4 | 0.6 | 1.74 | 0 | 34.4 | 29.0 | |
| | | | Site U1529 totals: | 5 | 46.4 | 2.46 | 5.30 | 0 | 46.4 | | 1.8 |
| U1530A | 34°51.6588′S | 179°03.4572′E | 1594.86 | 93 | 453.1 | 76.77 | 16.94 | 0 | 453.1 | 184.1 | |
| | | | Site U1530 totals: | 93 | 453.1 | 76.77 | 16.94 | 0 | 453.1 | | 7.7 |
| U1531A | 34°52.7767′S | 179°04.2241′E | 1354.87 | 1 | 15.0 | 1.0 | 6.67 | 0 | 15.0 | 51.5 | |
| U1531B | 34°52.7721′S | 179°04.2111′E | 1351.87 | 3 | 26.0 | 3.98 | 15.31 | 0 | 26.0 | 14.8 | |
| U1531C | 34°52.7239′S | 179°04.2586′E | 1306.87 | 3 | 28.4 | 2.25 | 7.92 | 0 | 28.4 | 23.5 | |
| U1531D | 34°52.7228′S | 179°04.2606′E | 1306.85 | NA | NA | NA | NA | 19.0 | 19.0 | 35.0 | |
| U1531E | 34°52.7591′S | 179°04.2344′E | 1355.01 | 8 | 21.7 | 0.79 | 3.64 | 17.9 | 39.6 | 139.5 | |
| | | | Site U1531 totals: | 15 | 91.1 | 8.02 | 8.80 | 36.9 | 128.0 | | 11.0 |
| | | | Expedition 376 totals: | 231 | 1244.0 | 222.37 | 17.88 | 351.2 | 1595.2 | | 54.6 |

Figure F7. Lithostratigraphic summary of Holes U1527A and U1527C on the rim of the caldera at the NW Caldera hydrothermal field. CSF-A = core depth below seafloor, Method A.

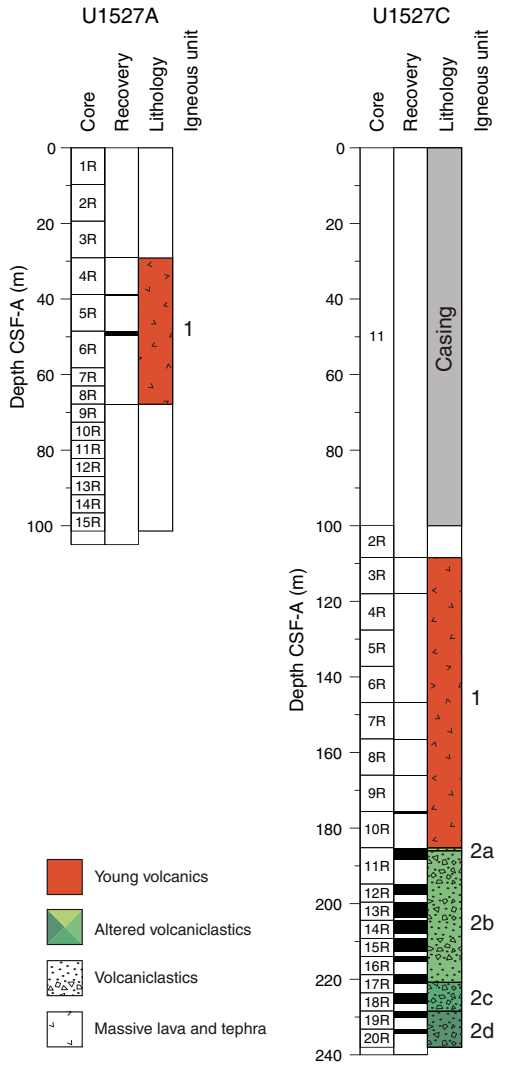


Figure F8. Distribution of alteration types and abundance of key minerals, Site U1527.

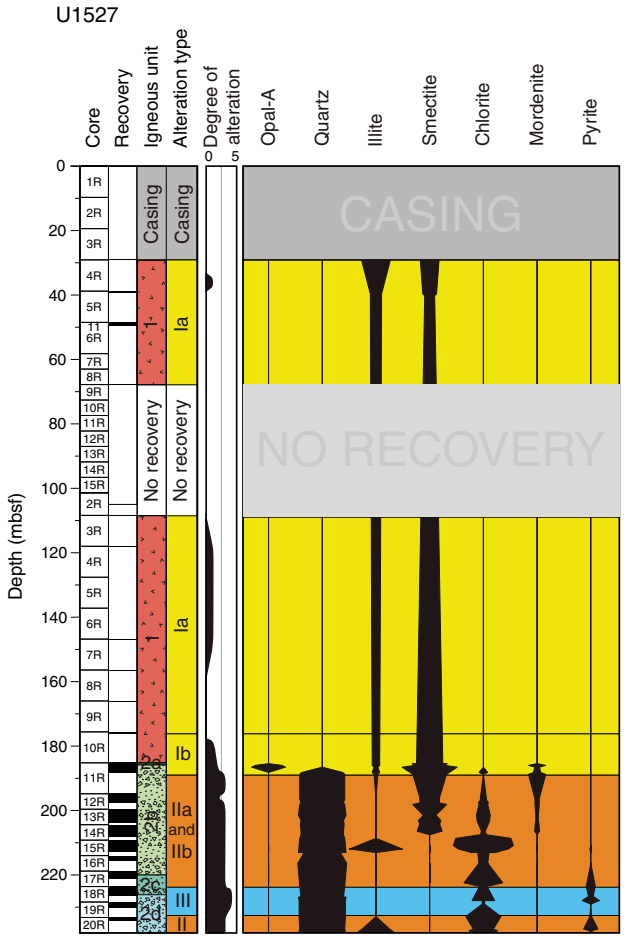


and clinopyroxene phenocrysts, but the degree of alteration in the matrix is higher compared to Subtype Ia. The alteration material in the matrix consists of Fe oxyhydroxide and illite with minor zeolite, smectite, magnetite, and pyrite.

Alteration Type II (185.72–234.38 mbsf) is characterized by more extensive alteration of most primary minerals, with the clasts and matrix of the volcaniclastic rocks being replaced by clay minerals, silica, and pyrite (Figure **F9**). This alteration type is also divided into two subtypes. Subtype IIa (185.72–234.38 mbsf; intercalated with Subtype IIb and Type III) features a pervasive green-gray chlorite-smectite mineral assemblage with increasing amounts of cryptocrystalline/amorphous silica infilling pore spaces and increasing abundance of disseminated pyrite with depth. Moderate to intense alteration occurs in both clasts and matrix of the primary volcaniclastic rocks and increases in intensity downhole. Subtype IIb (186.40–208.06 mbsf; intercalated with Subtype IIa) is characterized by several centimeter- to meter-scale zones of yellow-brown alteration overprinting greenish Subtype IIa. The overprinting boundary is sharp. Fe oxyhydroxide and occasionally oxidized pyrite give this alteration type its characteristic yellow-brown color. Throughout both the green and yellow-brown altered intervals, clasts display a range of degrees of alteration and resorption from slightly altered clasts with primary igneous textures and sharp boundaries to intensely altered clasts with diffuse boundaries to the surrounding matrix.

Alteration Type III (220.98–226.49 mbsf) represents a more heterogeneous alteration type that is intercalated with Subtype IIa. In this type of alteration, both clasts and matrix are pervasively altered (Figure **F9**). The matrix contains dark gray silica and chlorite, disseminated pyrite (as much as 3 vol%), and magnetite. Vugs are partially filled with clay minerals and silica.

Site U1527 is characterized by moderately to steeply dipping alteration boundaries, fractures, and faults in addition to shallowly dipping shears and relatively few veins. Alteration boundaries are sharp, dip between 0° and 74° (average and median = 48°), and demarcate the transition from Alteration Subtype IIa to Subtype IIb. Fractures also dip moderately to steeply, from 37° to 90° (average = 68°). The density of veins and fractures is low but increases slightly downhole. Fractures almost always have a brown/orange alteration halo overprinting all other types of alteration, which indicates late formation of fractures. The presence of brown/orange alteration along fractures and defining Subtype IIb may indicate the ingress of seawater through late-forming fractures. Faults are observed only in Hole U1527C, dip steeply (45°–83°; average = 66°), and are most abundant in Igneous Subunit 2c. All faults are discrete centimeter-scale zones with a normal sense of shear. Shallowly dipping shears

are defined by elongated ribbons of white clays that may represent flattened and altered volcanic clasts. White ribbons wrapped around larger volcanic clasts may indicate some crystal-plastic deformation. The shallowly dipping shears (average = 22°) are overprinted by higher angle brittle faults. The overall lack of veins and indication of late fracturing suggest that alteration is not structurally controlled and may instead be due to pervasive flow.

Figure F9. Representative intervals of alteration types, Hole U1527C. Type Ia: unaltered to slightly altered clast of dacite (376-U1527C-6R-1, 94–101 cm). Type Ib: dark unaltered clasts of dacite with well-defined boundaries surrounded by altered yellow-brown matrix (11R-1, 0–6 cm). Type IIa: pervasively altered clasts surrounded by chlorite-altered matrix (14R-2, 120–138 cm). Type IIb: overprint of IIb onto IIa (14R-2, 4–20 cm). Type III: pervasively altered clasts with resorbed, gradational boundaries (18R-1, 30–39 cm).

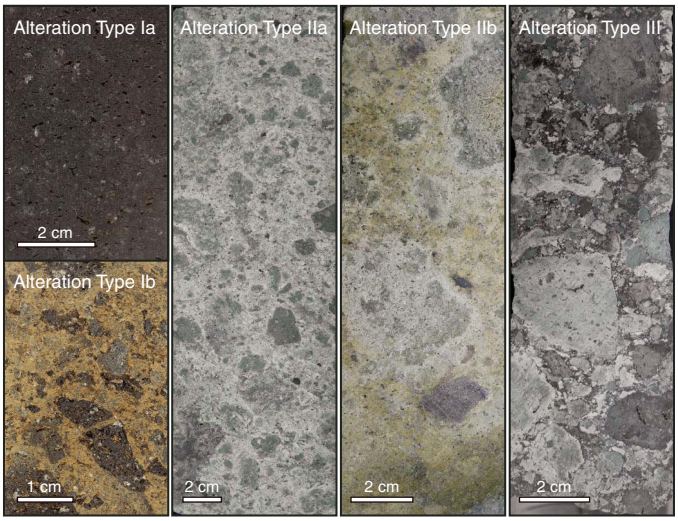


Unaltered volcanic rocks in Hole U1527A and the shallower sections of Hole U1527C (Igneous Unit 1) represent dacites that are compositionally similar to those previously reported from Brothers volcano (e.g., Haase et al., 2006; Wright and Gamble, 1999; Timm et al., 2012). Most of the pervasively altered volcaniclastic rocks recovered from Hole U1527C (Igneous Unit 2) share the incompatible element composition (i.e., Zr/Y and Zr/Ti) of overlying Igneous Unit 1 from the same hole. This suggests a common parental magma despite petrographic differences.

Geochemical analyses of the highly altered, variously colored volcaniclastic rocks demonstrate the mobility of alkali metals during high- and low-temperature hydrothermal alteration of the rock (Figure **F10**). Analyses of $K_2O$, Rb, Ba, MgO, and $SiO_2$ contents define a complex history of hydrothermal overprinting marked by multiple alteration stages. Alteration Type III displays significant enrichment in total sulfur content (as much as 1.9 wt%). Geochemical changes recorded in Hole U1527C are consistent with petrographic observations, including the formation of pyrite and replacement of groundmass and matrix by clay in deeper, more altered volcaniclastic rocks.

Organic carbon comprises the bulk of measured total carbon (TC) concentrations. Detectable only from 185 to 205 mbsf in Hole U1527C, this organic carbon may originate from seawater-derived fluid circulation and/or microbial biomass. Headspace analysis of pore space gases evolved from Hole U1527C hard rock samples indicates higher than ambient $H_2$ contents that may have been produced by mechanochemical sampling artifacts such as generation during RCB drilling and/or crushing rock samples prior to headspace sampling.

The two igneous units at Site U1527 have different natural remanent magnetization (NRM) intensities before demagnetization; samples from Igneous Unit 1 show more intense NRM (>0.5 A/m) than those from Igneous Unit 2. However, the direction of magnetization is consistent in both units, with an average inclination of

Figure F10. Variations of major element oxides compared with macroscopic estimate of degree of alteration, Holes U1527A and U1527C. Vertical lines = average values of shallower unaltered Igneous Unit 1 in Hole U1527A. Dashed lines = 1σ from average values. The two shallowest samples correspond to relatively unaltered volcanic material recovered from the BHA in Hole U1527C.

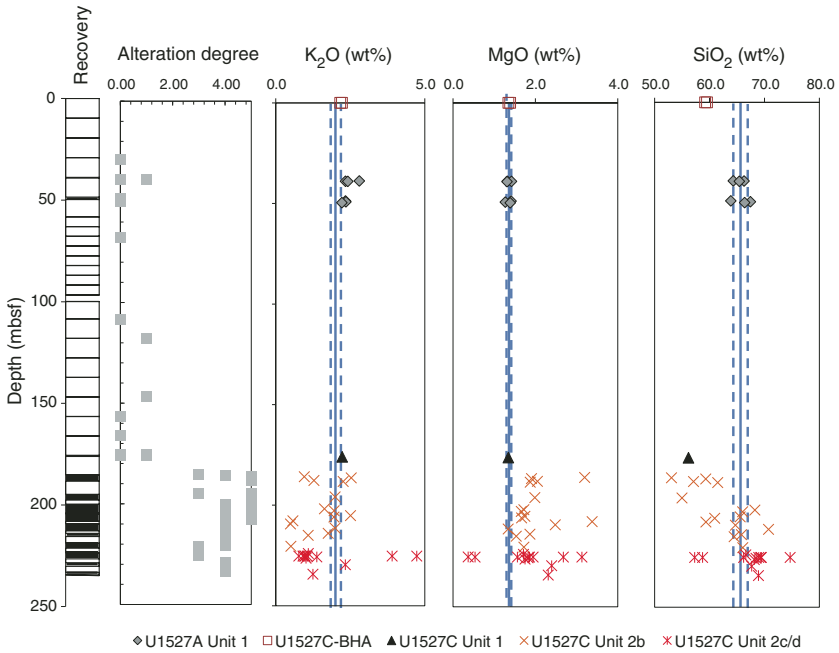

−59°, which is very close to the inclination of a geomagnetic axial dipole (GAD) of −55° at the latitude of Brothers volcano. This consistent GAD inclination suggests a young age for these rocks, most certainly from the current normal polarity Brunhes geomagnetic epoch. Igneous Unit 1 also has significantly larger magnetic coercivities than Igneous Unit 2. Thermal demagnetization experiments from Unit 2 show a more complex pattern compared to similar experiments from Igneous Unit 1 but indicate magnetite or titanomagnetite as the main magnetic mineral in both igneous units. In addition, susceptibility measurements and isothermal remanence magnetization (IRM) experiments suggest comparable magnetite content in both units, with a slight decrease in Subunits 2c and 2d.

The fresh dacitic volcanics of Igneous Unit 1 show an inverse correlation between porosity and bulk density, but no such correlation is observed between *P*-wave velocity and bulk density or *P*-wave velocity and porosity. Variably altered volcaniclastic rocks in Igneous Unit 2 display an inverse correlation between porosity and bulk density and between porosity and *P*-wave velocity. Mean bulk density (2.2 g/cm$^3$), porosity (30%), and *P*-wave velocity (3330 m/s) generally show small variations throughout Unit 2 and do not appear to be affected by transitions between alteration types. Alteration Subtypes IIa and IIb are clearly identifiable in reflectance colorimetry data. *P*-wave velocity sharply increases at the boundary between Subunits 2b and 2c (~4000 and 4200 m/s on section halves and discrete samples, respectively) followed by a downhole decrease in *P*-wave velocity to the bottom of Subunit 2c. In Subunit 2c, this variation in *P*-wave velocity is reflected in a similar trend in bulk density and matching inverse variation in porosity, which appears to be associated with deformation and shear in this unit.

Magnetic susceptibility measured on whole-round and section-half cores is consistent with discrete measurements. Magnetic susceptibility in Igneous Subunits 2a and 2b is overall higher than that in Subunits 2c and 2d. Thermal conductivity ranges from 1.09 to 2.35 W/(m·K) (average = 1.72 W/[m·K]); Igneous Unit 2 has higher values than Igneous Unit 1. Thermal conductivity in Igneous Unit 2 varies over smaller scales, reflecting changes in type and distribution of alteration minerals. Thermal conductivity is lower where alteration is dominated by the presence of water-rich clay minerals (e.g., low of 1.53 W/[m·K] in Subunit 2b at ~203.40 mbsf), whereas the highest thermal conductivity is observed along with increases in pyrite, silica, and magnetite concentrations in Subunit 2c. Hence, thermal conductivity data reflect the heterogeneity of mineral compositions and alteration assemblages throughout the core.

Five whole-round samples (each 11– 20 cm long) collected from hydrothermally altered, relatively hard materials in Hole U1527C (Table **T2**) were processed and preserved as subsamples for shore-based biological investigations that will include quantification of microbial and viral biomass, molecular analysis of the microbial communities from extracted DNA and RNA, estimation of microbial metabolic activity and viral production, and cultivation of subseafloor microbial components. Quantification of the perfluoromethyldecalin (PFMD) contamination tracer was conducted for the drilling fluid and the exterior and interior parts of whole-round samples. PFMD was routinely detected, although barely above detection levels, suggesting that penetration of drilling fluids to the interior of whole-round samples was minimal.

Table T2. Microbiological whole-round samples collected and preserved during Expedition 376. **Download table in CSV format.**

| Location | Hole | Samples (*N*) |
|---|---|---|
| NW Caldera (rim) | U1527C | 5 |
| Upper Cone | U1528A | 3 |
| Upper Cone | U1528C | 1 |
| Upper Cone | U1528D | 13 |
| NW Caldera (wall) | U1530A | 18 |
| Lower Cone | U1531C | 1 |

## Site U1528

### Background and objectives

Site U1528 (proposed Site UC-1A) is located inside a small (~40 m diameter at the top, ~25 m diameter at the bottom) pit crater at the summit of the Upper Cone of Brothers volcano at a water depth of 1228 m (Figure **F6**). The primary objective at this site was to drill into the upflow zone of the Type II hydrothermal system that is strongly influenced by magmatic degassing. In this area, discharge of relatively gas rich, very acidic fluids has resulted in advanced argillic alteration. Site U1528 addresses important Expedition 376 objectives related to the role of magmatically influenced hydrothermal fluids in transporting metals to the seafloor and provides a comparison of fluid–rock reactions with the Type I seawater-dominated hydrothermal system drilled at Sites U1527 and U1530.

### Operations

We conducted operations in four holes at Site U1528 (Table **T1**). Hole U1528A is located at 34°52.9177′S, 179°4.1070′E at a water depth of 1228.4 m. We used the RCB system to core from the seafloor to 84.4 mbsf and recovered 17.1 m (20%). The downhole conditions encountered in Hole U1528A dictated the need to deploy a reentry system to achieve our objectives.

Hole U1528B is located 10 m south of Hole U1528A at 34°52.9222′S, 179°4.1077′E at a water depth of 1229.4 m. Here, we drilled-in 10¾ inch casing to 24.3 mbsf, with the drilling assembly penetrating to 25.6 mbsf. We had trouble extracting the drilling assembly from the reentry system, which ultimately took several hours. Because of drilling-induced suspension of sediment in the seawater, visibility was limited and we could see only the top of the reentry funnel, observed to be at a water depth of 1224.8 m, which was consistent with it being properly set on the seafloor. After two separate unsuccessful attempts to reenter Hole U1528B with both the RCB system and the CDEX turbine-driven coring system (TDCS), we suspended operations. Further visual observations showed the reentry system was sitting at a slight angle that prevented the drill string from passing through the throat of the reentry funnel.

Our next objective was to perform the first offshore test of the TDCS. In Hole U1528C, located at 34°52.9215′S, 179°4.1128′E at a water depth of 1229.1 m, we drilled without coring using the TDCS to 22 mbsf and then cored to 53.5 mbsf, recovering 3.6 m (12%). Further advancement was prevented by a broken core barrel that remained in the TDCS bottom-hole assembly (BHA), forcing abandonment of Hole U1528C.

In Hole U1528D, located at 34°52.9219′S, 179°4.1164′E in the very limited flat central area of the pit crater and at a water depth of 1228.1 m, we drilled in 13⅜ inch (~35.2 cm) casing to 59.4 mbsf, with the drilling assembly penetrating to 61.3 mbsf. We then RCB cored to 359.3 mbsf and recovered 87.2 m (29%) under good hole conditions. After the bit reached 40 h of rotation time, when it would normally be changed before continuing to core, we instead decided to take downhole temperature measurements and obtain borehole fluid samples in the open hole through the existing bit.

The Elevated Borehole Temperature Sensor (ETBS) memory tool was deployed first and recorded a maximum temperature of 35°C at 357 mbsf, which was 2 m above the drilled bottom of the hole. The subsequent deployment of the 1000 mL Kuster Flow-Through Sampler (FTS) tool ended with its failure under compression in the open hole. We then made an unsuccessful attempt to recover the tool with a fishing tool BHA equipped with boot-type junk baskets. Reentry into Hole U1528D was complicated by a plume emanating from the reentry funnel. We next deployed a logging BHA, lowered the backup 600 mL Kuster FTS tool on the core line, and successfully recovered a fluid sample from 279 mbsf. A subsequent ETBS downhole temperature measurement at the same depth recorded a maximum temperature of 212°C, confirming that the flasked wireline high-temperature triple combo (HTTC) logging tool string (natural gamma radiation [NGR], litho-density, and temperature tools) could be deployed. We successfully performed two upward logging passes from 323 mbsf. Another deployment of the 600 mL Kuster FTS tool then recovered a second borehole fluid sample from 313 mbsf; subsequent deployment of the ETBS memory tool recorded a maximum temperature of 165°C (following cold seawater circulation). Next, we drilled down with a tricone bit BHA to clean out the hole to 356 mbsf, which was the depth of the top of the lost 1000 mL Kuster FTS tool.

A concave mill bit and two boot-type junk baskets were then deployed to attempt to remove the remaining parts of the lost 1000 mL Kuster FTS tool. After reentering Hole U1528D for the sixth time and despite very poor visibility around the reentry funnel, we advanced the mill bit to the bottom of the hole at 359.3 mbsf. Upon recovery, there was no evidence of the 1000 mL Kuster FTS tool in the boot baskets. The next fishing attempt used the reverse-circulation junk basket (RCJB) assembled in conjunction with the boot-type junk baskets. After the seventh reentry of Hole U1528D, we worked the RCJB BHA back to bottom (359.3 mbsf), where we circulated 25 bbl of high-viscosity mud for ~15 min while working the RCJB up and down. When the end of the drill string cleared the rig floor, the discovery that the lowermost 172.8 m was missing ended Hole U1528D drilling operations. The drill string failed in a piece of 5 inch pipe above the BHA. The recovered broken piece showed significant damage directly attributable to the corrosive downhole environment.

Upon completion of coring operations at Site U1531, we returned to Hole U1528D (~3 weeks later) to conduct a series of alternating downhole temperature measurements using both the ETBS memory tool and Petrospec spool-in thermocouple memory tool (TCMT) and two 600 mL Kuster FTS tool deployments that resulted in recovering a borehole fluid sample from 160 mbsf. Two successful temperature measurement runs recorded maximum temperatures of 198°C (ETBS) at 195 mbsf and 156°C (TCMT) at 160 mbsf. Site U1528 operations concluded with successful recovery of the failed Hole U1528B reentry system at the end of Expedition 376. In total, 568.9 h, or 23.7 days, were spent at Site U1528.

## Principal results

Rocks cored at Site U1528 are divided into three igneous units (Figure **F11**). Igneous Unit 1, recovered in Holes U1528A (0–6.03 mbsf) and U1528C (26.50–31.41 mbsf), consists of polymict lapilli tephra made up of subangular to subrounded volcanic clasts that have experienced varying degrees of alteration. Igneous Unit 2, recovered in Holes U1528A (16.30–83.57 mbsf), U1528C (35.50–46.00 mbsf), and U1528D (61.30–269.30 mbsf), is divided into three subunits based on internal rock fabric and the presence of primary minerals. Subunits 2a and 2c are composed of sequences of altered lapillistones and lapilli-tuffs with subordinate intervals of altered tuffs and tuff-breccias. Clasts are volcanic in origin and altered to differing degrees; the matrix consists of secondary mineral assemblages. Identification of original lithologies becomes increasingly difficult with depth (especially in Subunit 2c). More coherent, massive dacite lava, affected by a lesser degree of alteration, occur between 152.90 and 160.17 mbsf and make up Subunit 2b. Igneous Unit 3, recovered exclusively in Hole U1528D (162.50–269.03 mbsf), consists of altered dacite lava with some relatively unaltered intervals.

The dacitic pyroclastic rocks and lavas at Site U1528 are pervasively altered yet still show distinct similarities in petrography and whole-rock geochemistry to unaltered volcanic materials encountered in Igneous Unit 1 at Sites U1527, U1529, and U1531 and to published descriptions and geochemical results for unaltered dacite recovered elsewhere at Brothers volcano (e.g., Haase et al., 2006;

Figure F11. Lithostratigraphic summary of Holes U1528A, U1528B, and U1528D in the pit crater of the Upper Cone.

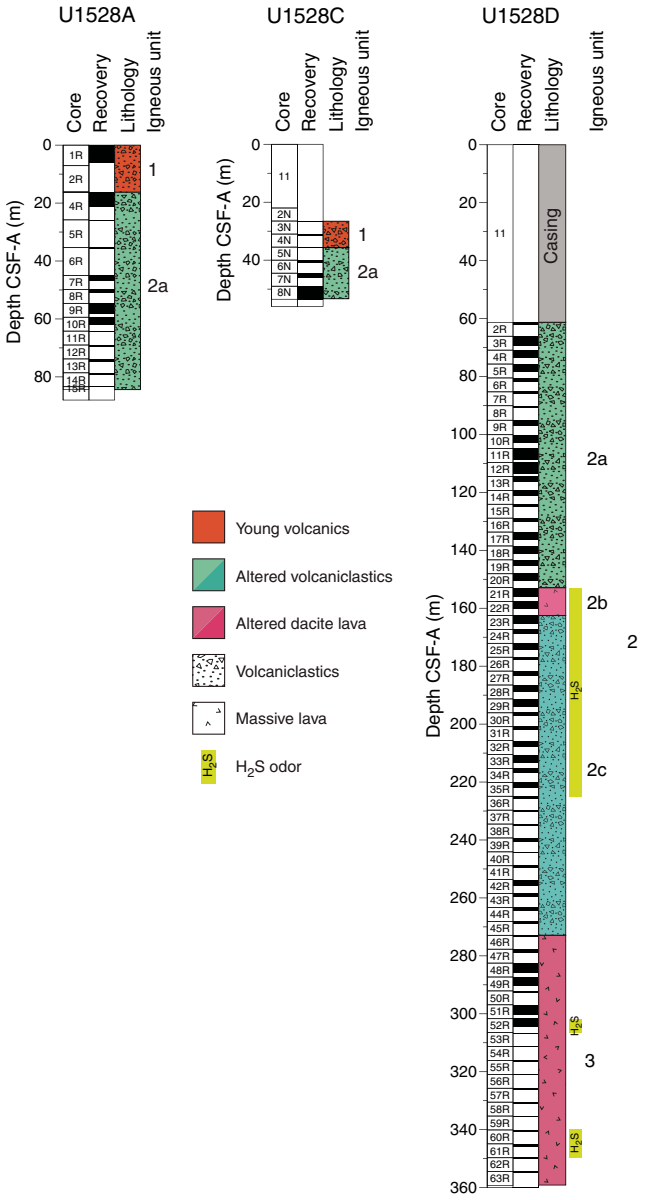

Wright and Gamble, 1999; Timm et al., 2012). Even though intervals with (partially) unaltered phenocrysts are rare, primary igneous textures such as vesicles and the crystal shapes of plagioclase and (rarely) pyroxene phenocrysts and microlites, now infilled and replaced by secondary minerals, can be recognized in most samples. Petrography and the abundance of elements that are less affected by alteration suggest that the Site U1528 protolith was dacitic tephra and lava similar to that previously encountered at Brothers volcano.

Four distinct alteration types are observed in core material recovered from Site U1528 (Figure **F12**). Alteration Type I (0–35.9 mbsf), classified as slightly altered, occurs in unconsolidated gravels. The dominant alteration mineral assemblage consists of smectite with minor pyrite, opal, natroalunite, pyrophyllite, and native sulfur. Two distinct volcanic clast colors are observed: dark gray clasts, which contain more smectite, and light gray clasts. Native sulfur occurs in crystalline tabular (orthorhombic) and globular grain morphologies.

Alteration Type II (classified as highly altered) occurs in several intervals throughout Site U1528 (e.g., 148.1–154.4 mbsf) and is characterized by an alteration mineral assemblage of illite, smectite, opal, quartz, pyrite, and anhydrite. Alteration is typically blue-gray in color, manifests by brecciation, and exhibits relict perlitic texture (Figure **F13**). Plagioclase phenocrysts are variably pseudomorphed by natroalunite and anhydrite, whereas pyroxene is pseudomorphed by anhydrite, smectite, and pyrite. The latter is abundant (average = 1–5 vol%) and occurs not only in pyroxene pseudomorphs but also as subhedral to euhedral disseminated grains and in discrete veins associated with anhydrite. Primary titanomagnetite is rimmed and shows progressive replacement by pyrite that exhibits skeletal texture and contains abundant anhydrite inclusions.

Alteration Type III, classified as highly to intensely altered, is intercalated with Type II (e.g., 239.3–264. 5 mbsf), and the boundary between these alteration types can be either gradational or sharp. Type III is represented by pervasively altered white-gray volcaniclastic rocks (Figure **F13**). A mineral assemblage of natroalunite, pyrophyllite, and rutile with lesser quartz, opal, smectite, pyrite, and anhydrite, characterizes Type III. Natroalunite, pyrophyllite, and silica are more abundant in the matrix, whereas smectite is enriched

Figure F12. Distribution of alteration types and abundance of key minerals, Site U1528. MS = magnetic susceptibility, WRMSL = Whole-Round Multisensor Logger.

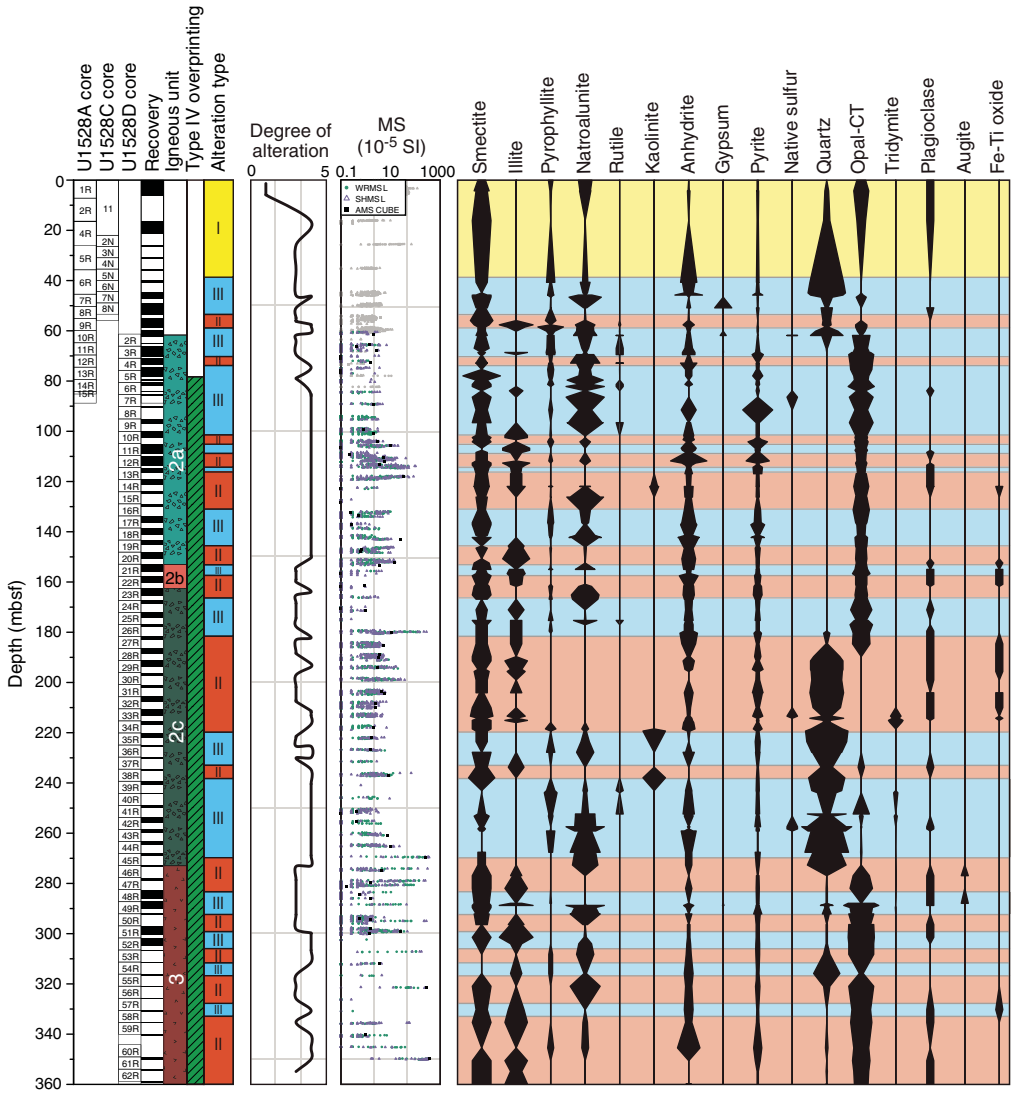

Figure F13. Representative intervals of alteration types, Site U1528. A. Type I (376-U1528A-1R-3, 25–38 cm). B. Type II (376-U1528D-22R-1, 91–103 cm). C. Type III (4R-2, 94–102 cm). D. Type IV. Top: Type IV crosscutting Type II (10R-1, 71–76 cm). Bottom: Type IV crosscutting Type III (18R-2, 71–77 cm).

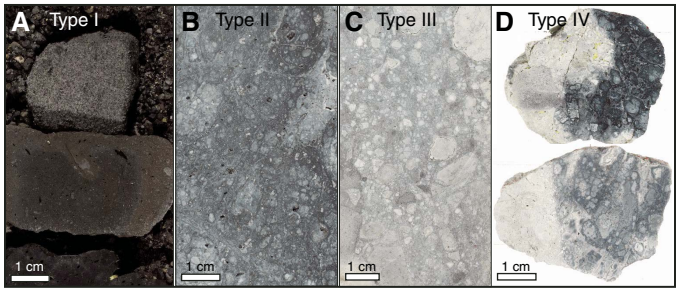


in clast material. Plagioclase and pyroxene are completely pseudomorphed by natroalunite, anhydrite, and pyrite. Late-stage anhydrite-pyrite veins commonly cut pseudomorphed plagioclase crystals. Titanomagnetite is almost completely replaced with leucoxene and pyrite. Vugs are infilled with anhydrite and minor pyrite, native sulfur, natroalunite, and silica. In addition, fine-grained pyrite is finely disseminated throughout matrix and clasts.

Alteration Type IV is defined by discrete to diffuse white veins that cut and postdate Types II and III. Type IV is first observed at 77.2 mbsf and occurs until the cored bottom of Hole U1528D at 355.1 mbsf. It is characterized by an alteration assemblage of natroalunite, anhydrite, rutile, quartz, opal, native sulfur, and pyrophyllite (Figure **F13**). Mineralogically, Type IV is distinguished from Types II and III by higher abundances of native sulfur, silica, and rutile. This alteration type occurs as discrete white veins and distinct alteration halos typically <1 cm but occasionally as wide as 4 cm and commonly with a vuggy texture, overprinting previous alteration and often preserving earlier alteration textures. Pyrite is generally absent or oxidized to Fe oxyhydroxides within the halos, and native sulfur is the major mineral phase infilling vugs.

Fluid inclusions in the most recent vug and vein crystals of anhydrite, quartz, natroalunite, and gypsum indicate that the hydrothermal system at Site U1528 is highly dynamic. Two dominant fluid types are variably involved in fluid-rock interactions (Figure **F14**): a buoyant, hot (220°–360°C), sulfur-rich, acidic hypersaline brine (NaCl > 30 wt%) and hot modified seawater. A massive influx of seawater (NaCl = 3.5 wt%) locally overwhelmed the hypersaline brine along fractures or pervasively diffused into the hot formation, where it is heated to temperatures of 55°–360°C. Fluid inclusion salinities plot into two separate regions: (1) at or near seawater compositions and (2) as a hypersaline brine at or along the NaCl saturation curve. Both regions are attributed to depressurization in the formation caused by sudden fracturing events, resulting in phase separation (Figure **F14**). This process gives rise to a more saline, higher density fluid for both hypersaline brine and seawater and, at the same time, forms a low-density vapor phase that condenses through cooling to a low-salinity aqueous solution under subcritical conditions.

Structures that occur across Holes U1528A, U1528C, and U1528D include volcanic fabrics, alteration veins, and fractures. Volcanic fabrics are best observed in Holes U1528A and U1528D and are defined by vesicles and plagioclase microlites (primary and altered) and, to a lesser extent, phenocrysts. Volcanic fabrics have two forms, those in volcanic clasts and those in coherent lavas. Vol-

Figure F14. Salinity (NaCl equivalent wt%) vs. homogenization temperature and corresponding enthalpy of NaCl-$H_2O$ (Bischoff and Rosenbauer, 1985) for fluid inclusions from anhydrite, gypsum, and natroalunite recovered from Site U1528. NaCl saturation curve calculated from Driesner and Heinrich (2007), and NaCl vapor conjugate curve calculated from Bischoff (1991). Phase separation (boiling) curves calculated for seawater (bc1), seawater (sw) + 0.22 m $CO_2$ (bc2), 33 wt% NaCl equivalent hypersaline brine (bc3), and 33 wt% NaCl equivalent hypersaline brine + 0.22 m $CO_2$. Broken line with arrow = salinities caused by vapor condensation under subcritical conditions.

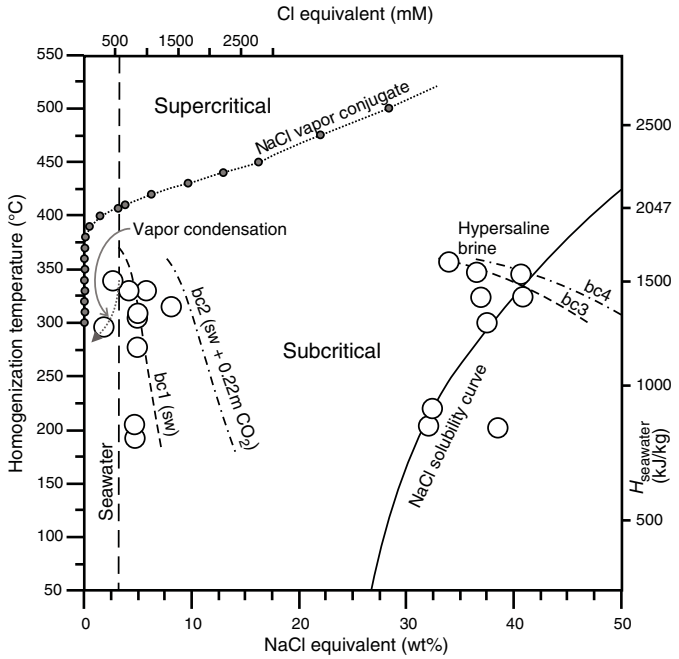


canic fabrics within clasts can be weak to strong, but each clast has a distinct orientation, suggesting brecciation after fabric formation. Fabrics over continuous intervals (i.e., lavas) have a similar orientation and tend to dip >45°. Peaks in volcanic fabric intensity are observed in Igneous Subunit 2b and Igneous Unit 3 in Hole U1528D.

Alteration veins occur throughout Holes U1528A and U1528D across all igneous units and alteration types. Veins are most commonly filled by anhydrite, pyrite, silica, and native sulfur and are typically uniform but can be vuggy; some have halos. The presence of halos is the basis for Alteration Type IV. Vein density peaks between 100 and 190 mbsf, which is coincident with a peak in native sulfur, vuggy veins, and a deviation in borehole temperature. Vein dip varies from horizontal to vertical, with an average of ~60° in both holes. The distribution of dips downhole is variable: a few zones have a large range in dip (e.g., 0°–90°) and other zones have dips >45°. Vein thickness ranges from 0.05 to 1 cm and averages ~0.2 cm. Vein thickness is variable downhole, but it appears to increase in intervals with a large range of vein dip, and thicker veins tend to have steeper dips.

Fractures are observed in all three holes, but their abundance is limited. Fractures in Hole U1528C are irregular and lined with native S. Native S is more abundant where the fractures are irregular. In Hole U1528D, fractures are typically clustered in the uppermost 175 m of the hole and have steeper dips (i.e., >60°). Fracture density has three peaks; the one near 290 mbsf coincides with a deviation in borehole temperature and a large range in vein dip.

Geochemical analysis of 75 powders from Hole U1528D was performed via inductively coupled plasma-atomic emission spec-

Figure F15. Variations in major element oxides, Site U1528. Horizontal dashed lines = depth intervals marked by major geochemical changes and alteration types. Vertical shaded area = compositional range (and 2σ from the average) for fresh dacites from Igneous Unit 1 in Hole U1527A and at Site U1529. Data are from ICP-AES analyses, except those with plus symbols, which are handheld portable X-ray fluorescence (pXRF)-generated data.

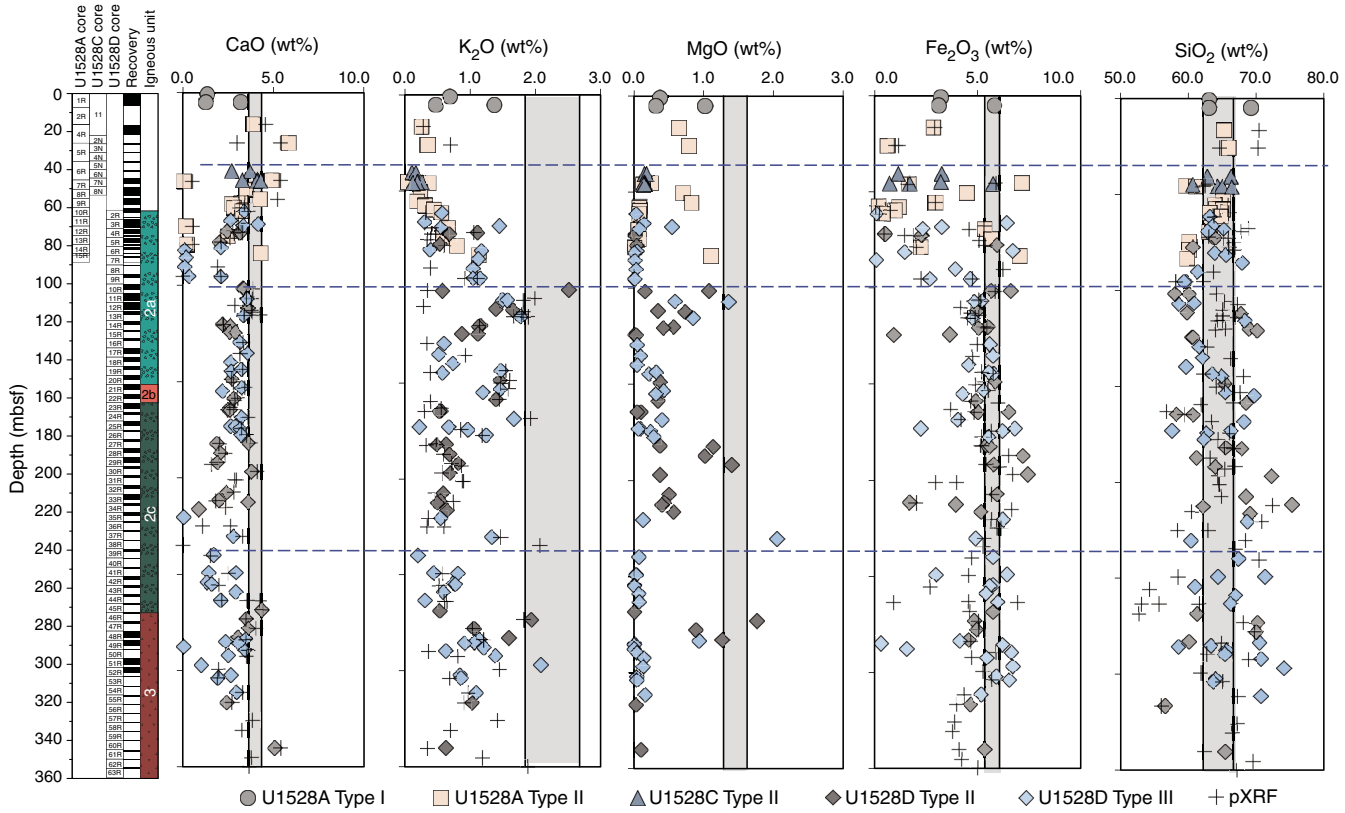


troscopy (ICP-AES) for major, minor, and trace elements and via elemental analysis for TC, total nitrogen (TN), and total sulfur. Results of these analyses were used to define major geochemical changes during hydrothermal fluid-seawater-rock interactions in Hole U1528D. Variable extents of depletion in alkalis (K and Na), Mg, Fe, and Mn and strong enrichment in total sulfur (as much as 15 wt%) occur throughout the hole. In Igneous Unit 1, Zr/Ti values range from 30.0 to 31.3 mg/g and are indistinguishable from average Zr/Ti values for Unit 1 in Hole U1527A and at Site U1529 (i.e., 30.5–32.3 mg/g). This similarity suggests that the upper lava and tephra units recovered at Sites U1527–U1529 may derive from similar parental magmas. Considering that Y is relatively mobile under hydrothermal conditions in contrast to Zr, the Y/Zr value of altered volcaniclastics is used as a tracer for the extent of alteration. Two main intervals are characterized by lower Y/Zr value (i.e., relative to unaltered dacite from Brothers volcano): (1) 46–95.5 mbsf in Igneous Subunit 2a, dominated by Alteration Type III, and (2) 240–325 mbsf overlapping Subunit 2c and Igneous Unit 3 and associated alternating Types II and III. Variable extents of depletion in alkalis (K, Rb, and Na), Mg, Ca, and Fe and strong enrichment in total S (as much as 15 wt%) occur throughout the hole (Figure **F15**). Based on average compositions of discrete intervals throughout the entire 360 m section in Hole U1528D, we estimate that >75% of both Mn and Mg have been lost because of hydrothermal alteration. Other significantly depleted elements include a >50% loss of Na, K, and Rb and a >30% loss of Ca and P. Total S contents vary between 2.1 and 15.1 wt% because of the formation of S-dominated secondary minerals (e.g., natroalunite, native S, pyrite, and anhydrite); anhydrite represents a significant component of the total S inventory (~22% on average). Fe appears to be strongly depleted in late-stage Type IV alteration, suggesting that pH, $fO_2$, and $fS_2$ conditions changed substantially from Types II and III, leading to extensive loss of Fe in possibly $\Sigma SO_4$-rich but $\Sigma H_2S$-poor hydrothermal fluids. Similar to Site U1527, organic carbon comprises the bulk of measured TC content but remains very low, yielding an average of ~250 µg/g at Site U1528.

One sample of interstitial water (376-U1528C-7N-1, 140–150 cm) recovered from 45.9 mbsf has a low pH of 4.1, which is consistent with the presence of acidic magmatic fluids. Nearly equimolar enrichments in Ca and $\Sigma SO_4$ suggest that dissolution of anhydrite at low temperatures may be occurring in the pore water.

Three borehole fluid samples were collected from Hole U1528D using the 600 mL Kuster FTS tool at ~279 and ~313 mbsf and then 23 days later at 160 mbsf. Estimated temperatures of 212° and >236°C for the first two samples and 140°C for the later sample were determined by downhole logging. The fluids have nearly identical Cl, Br, and Mg concentrations, and Na concentrations are all lower than seawater. Highly elevated $\Sigma SO_4$ and very acidic pH values (as low as 1.8) are characteristic of acid-sulfate fluid. Results indicate that the low-salinity borehole fluids are not derived from phase separation of circulating seawater but rather that they acquired their geochemical signatures through the direct input of magmatic fluids to unaltered seawater at temperatures of at least 350°C. During fluid origin and upflow, Mg and K are removed from rock and added to

fluids during fluid-rock reaction, which is balanced by a net removal of $\Sigma SO_4$, Ca, and Sr from the fluids into secondary minerals, primarily as natroalunite and/or anhydrite.

Gas pore space components, including $H_2$, $\Sigma CO_2$, and acid-volatile S, are elevated over ambient atmospheric levels. These anomalies may derive from subseafloor hydrothermal input of volatile-rich fluids that share similar chemical properties with the seafloor hydrothermal fluids discharging at the Upper and Lower Cone sites.

Eighty-three archive halves were measured for NRM and underwent alternating field (AF) demagnetization experiments using the cryogenic magnetometer. The sections show generally low NRM intensities where the largest pieces have primary magnetization components (after AF steps of 20 mT) with negative inclinations, suggesting normal polarities. AF and thermal demagnetization experiments on 82 discrete samples from Igneous Units 2 and 3 were also carried out. The drilling-induced overprint is generally removed after 20 mT AF demagnetization on the discrete samples, leaving, in most cases, a stable primary magnetization. The two igneous units have very low NRM intensities, which is in agreement with the observations from the cryogenic magnetometer. Both units show a consistent direction of magnetization with average inclination compatible with the inclination of a GAD of −55° at the present-day latitude of Brothers volcano. This consistent GAD inclination suggests a coherent young age for these rocks, most certainly representing the current normal polarity Brunhes geomagnetic epoch. Thermal demagnetization experiments from these units show a complex pattern, suggesting irreversible transformation of magnetic minerals during heating to >400°C; this transformation is confirmed by changes in the magnetic susceptibilities measured with the AGICO Kappabridge susceptibility meter before and after heating. In addition, IRM experiments suggest that these rocks contain minerals with large magnetic coercivities, such as titanohematite, in addition to titanomagnetite.

Physical property measurements for Igneous Unit 1 (Alteration Type I) are consistent with the ranges expected for fresh unconsolidated dacitic volcaniclastics. In Igneous Units 2 and 3, more complex variations in physical properties associated with igneous unit and/or alteration type are observed. For example, magnetic susceptibility is generally higher in intervals of Alteration Type II than Type III (Figure **F12**), which may be explained by the observed partial replacement of titanomagnetite by rutile and pyrite in the relatively more altered rocks of Type III. Downhole measurements also indicate an association between Type II and increases in NGR attributed to $^{40}K$; however, this association could not be confirmed by NGR measurements in the laboratory because of the recovered core material was fragmented. The relatively high $^{40}K$ NGR signal identified in a core from Type III alteration (Section 376-U1528D-48R-1) is consistent with this observation.

The boundary between Igneous Units 2 and 3 is clearly defined by changes in grain density, bulk density, porosity, *P*-wave velocity, and thermal conductivity and by an increase in magnetic susceptibility. By contrast, boundaries between igneous subunits within Igneous Unit 2 are less clearly defined by variations in physical properties. An interval of relatively lower bulk density and *P*-wave velocity and higher porosity is observed between ~145 and ~220 mbsf but is not associated with a defined igneous subunit or alteration type boundary. Instead, this interval corresponds to the depth at which $H_2S$ gas was smelled during core splitting, and its boundaries correspond to a borehole temperature anomaly and increased fracture densities, vein thicknesses, and range of vein dip.

A series of downhole measurements was conducted and borehole fluid was sampled at the end of Hole U1528D coring operations. Three runs of the ETBS memory tool were completed in Hole U1258D. The first deployment, made prior to logging to help determine which logging tools could be deployed, measured an average temperature of 33°C at 357 mbsf.

A high-temperature flasked wireline logging string consisting of litho-density, NGR, and logging head temperature tools was run to 332 mbsf in Hole U1528D. Variations in the total NGR measurements are mostly related to peaks in K, generally correlated to Alteration Type II, which is rich in illite. Overall, the downhole density log correlates well with bulk density measured on the core samples and shows trends that are generally correlated with igneous units and subunits:

- From 65 to 145 mbsf (Igneous Subunit 2a), density gradually decreases downhole;
- From 145 to 250 mbsf, density decreases sharply (between 140 and 155 mbsf; Subunit 2b) followed by a gradual increase with depth (Subunit 2c); and
- From 250 to 330 mbsf, density is very variable (Igneous Unit 3).

Downhole caliper measurements revealed three zones of washouts where the borehole diameter exceeded 33.0 cm (13 inches) and reached up to 43.2 cm (17 inches): 149–162, 195–210, and 297–324 mbsf. The median diameter was determined to be 28.5 cm (11.2 inches), which only slightly exceeds the drill bit diameter of 25.1 cm (9⅞ inches). Two bridges were encountered on top (292 mbsf) and at the bottom (323 mbsf) of the deepest washout interval while lowering the logging tool string.

The three temperature profiles acquired during wireline logging suggest a convective temperature regime with small temperature increases at ~100 and 150 mbsf and larger increases at ~275 and 295 mbsf. A temperature reversal (i.e., a decrease in temperature with depth) is observed at ~250–260 mbsf. Over the 2.5 h of logging, the temperature increased by ~8°C in the isothermal zones and by 24.5°C between 270 and 310 mbsf, reaching 247°C. This increase suggests that the downhole temperatures had not yet reached equilibrium. The temperature anomalies at ~150 and ~295 mbsf are accompanied by increases in borehole diameter, peaks in K, the first instance of $H_2S$ odor emanating from the cores, native S observed in veins, high fracture density with varied fracture dips, crosscutting fractures, and increased vein density. These zones are interpreted to be structurally controlled permeable intervals.

In total, 3, 1, and 13 whole-round samples (3–16 cm long) were collected from Holes U1528A, U1528C, and U1528D, respectively, for microbiological analyses (Table **T2**). The sampled lithologies represent the various igneous units recovered. Samples were processed for shore-based DNA and RNA analyses, cell and viral counting, and viral and microbial activity measurements. All samples were analyzed on board for adenosine triphosphate (ATP) concentration; two samples gave positive values. The other samples contained compounds that inhibited the enzyme, luciferase, used for the ATP test. Nutrient addition bioassays with inorganic N and P, or organic carbon, were initiated to determine the nutritional constraints on biomass in this environment. PFMD was used for contamination testing. PFMD was usually detected on the outside of uncleaned cores and, on rare occasions, was above detection levels on the cleaned outside of cores. However, it was usually below detection on the inside of cores, indicating that penetration of drilling fluid to the interior of whole-round drill cores (where we collected samples) is unlikely.

# Site U1529

## Background and objectives

Site U1529 (proposed Site WC-1A) is located on the western side of the caldera floor of Brothers volcano at a water depth of 1765 m (Figure **F6**). The primary objective for this site was to drill a second hole (the first was at Site U1527) into the margin of the upflow zone of a hydrothermal system dominated by modified seawater-derived fluids. This site was planned to penetrate deeper into the hydrothermal system and obtain a record of the recent eruptive history in the caldera.

## Operations

We conducted operations in two holes at Site U1529 (Table **T1**). Hole U1529A is located at 34°52.5161′S, 179°3.5139′E at a water depth of 1735.0 m. We used the RCB system to core from the seafloor to 12.0 mbsf, with poor recovery of 1.86 m (16%). The downhole conditions encountered in Hole U1529A were extremely difficult because of the unconsolidated volcaniclastic material, which caused high torque and tight hole conditions that ended drilling this hole. In Hole U1529B, located at 34°52.5217′S, 179°3.5207′E at a water depth of 1733.0 m, RCB coring under similarly difficult hole conditions penetrated to only 34.4 mbsf, with very poor recovery of 0.6 m (1.7%). After observing a tight hole, we attempted to work the drill string back to ~15 mbsf but lost circulation because the bit and jets were plugged with volcaniclastic material. This loss of circulation resulted in abandonment of Hole U1529B. An 8.2 m long ghost core was recovered from the core barrel that was in place while working the drill string out of the hole. In total, 44.0 h, or 1.8 days, were spent at Site U1529.

## Principal results

A single igneous unit was recovered from Holes U1529A (0–2.52 mbsf) and U1529B (0–24.82 mbsf). Igneous Unit 1 consists of decimeter-thick alternating intervals of unaltered, black plagioclase-pyroxene-phyric dacite lava and unconsolidated, black monomict lapilli tephra (Figure **F16**). The contacts between the lavas and the tephra were not recovered. The moderately vesicular (~10 vol%) lava was recovered as individual pieces that are 0.5–6 cm long. The lava has a hypohyaline texture with groundmass rich in flow-aligned plagioclase microlites and shows fine fracture networks indicative of incipient breakup. The lapilli tephra consists of fine ash– to medium lapilli–sized angular to subangular fragments of dacite lava and fragments of plagioclase and pyroxene crystals. Dacite lavas at Site U1529 resemble the dacites recovered at Site U1527.

The ghost core from Hole U1529B, which contains material from anywhere between 0 and 34.4 mbsf, similarly consists of unconsolidated, unaltered, black lapilli-ash ranging in size from ash to medium lapilli. Ash- and lapilli-sized clasts are subangular and angular with a vesicularity and mineral assemblage (plagioclase-clinopyroxene phenocrysts and glomerocrysts) consistent with the lapilli tephra being a mixture of Igneous Unit 1 volcanic rocks.

The volcanic rocks of Igneous Unit 1 appear unaltered to slightly altered. Alteration Type I is the only alteration type recognized at this site and occurs within the lapilli tephra and coarser fragments of dacite lava. The alteration type is defined by the presence of minor smectite and Fe oxyhydroxide replacing phenocrysts and groundmass and lining some vesicles. A few individual clasts in Unit 1 are more strongly altered and contain microcrystalline silica, Fe oxyhydroxide, and a green clay mineral.

Figure F16. Representative macroscopic samples from the single igneous unit at Site U1529. A. Volcaniclastic xenocryst included in dacite lava. B, C. Dacite with fractures accentuated by white halite. D. Lapilli-sized fragments of dacite lava.

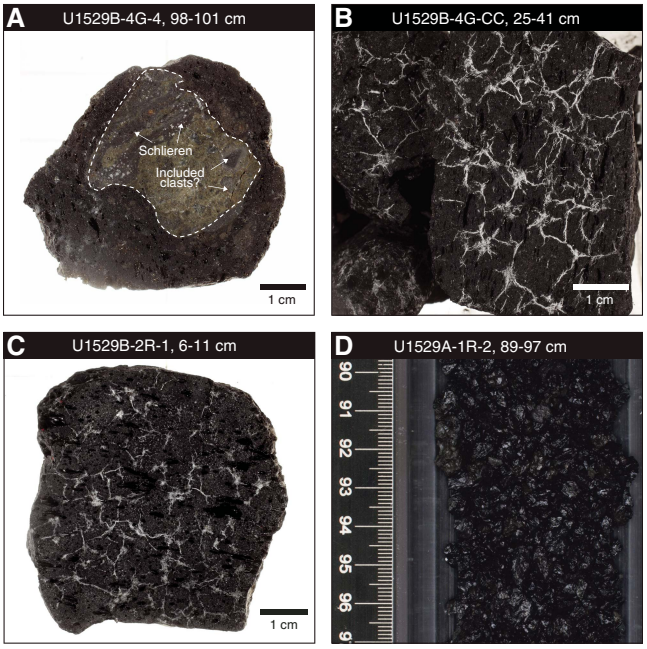


At Site U1529, no meaningful structural measurements could be made because no pieces of oriented core were recovered. Some pieces of dacite have a network of microfractures, but no faults or alteration veins are present. In both Holes U1529A and U1529B, the main structure observed is a shape-preferred orientation defined macroscopically by vesicles and microscopically by vesicles, phenocrysts, and microlites.

Unaltered to slightly altered clasts and lapilli from Igneous Unit 1 are typical dacites, with $SiO_2$ content ranging from 62.3 to 65.4 wt% and $Na_2O + K_2O$ content varying from 6.61 to 7.07 wt%. These dacites are similar in major element composition to unaltered dacites at Site U1527 and consistent with the small compositional range previously reported for dacites at Brothers volcano (e.g., Haase et al., 2006; Wright and Gamble, 1999; Timm et al., 2012).

The uppermost sample (0.06 mbsf) from Hole U1529A and two samples from the ghost core have lower values of TC (<200 µg/g) compared with the other five samples from this hole, for which TC ranges from 221 to 344 µg/g. Total S contents are <220 µg/g, which is consistent with total S abundances previously reported from Brothers volcano. Total N and total inorganic carbon are below the limit of detection in all Site U1529 samples.

No paleomagnetic measurements were performed on the samples from Site U1529 because of the absence of any oriented core pieces. Moreover, the low recovery and fragmented nature of the clasts and volcaniclastic sediments made the cores mostly unsuitable for continuous physical property measurements on whole-round cores and section halves. However, NGR measurements for Hole U1529A recorded values of ~13 counts/s (1.9 mbsf), and Section-Half Multisensor Logger (SHMSL) point data indicate magnetic susceptibilities as high as ~2250 × $10^{-5}$ IU (15.14 mbsf).

Five discrete samples from Hole U1529A and three samples from Hole U1529B, including cut clasts and volcaniclastics, were

analyzed for moisture and density. Bulk density ranges from 1.92 to 2.37 g/cm$^3$, whereas grain density ranges from 2.43 to 2.50 g/cm$^3$. Porosity varies from 6 to 38 vol% and is inversely correlated with bulk density. Three measurements of *P*-wave velocity made in the *x*-direction on coherent clasts in section halves of Hole U1529A vary from ~3500 to 4500 m/s. No thermal conductivity measurements were made because of the limited recovery and fragmented nature of the material.

No samples were collected from Site U1529 for microbiological analyses because of the nature of the recovered material.

## Site U1530

### Background and objectives

Site U1530 (proposed Site NWC-3A) is located on a narrow bench on the NW Caldera site of Brothers volcano at a water depth of 1595 m (Figure **F6**). The primary objective at this site was to drill through the lower part of the Alteration Type I hydrothermal system. Site U1530 is located ~400 m east of Site U1527 on a ~30 m long by ~10 m wide bench toward the upper part of the NW Caldera wall and is structurally above a known prominent metal-rich stockwork zone. The operations plan at Site U1530 was to penetrate ~450 m through the upper stockwork and then into deeper portions of the inferred hydrothermal upflow zone and continue through a thicker stratigraphic section of lavas in the caldera, hoping to intersect the footwall of the original caldera. Intersection of the stockwork was expected to provide the best opportunity to investigate the transport of metals through the Brothers volcano hydrothermal system.

### Operations

Operations were conducted in one hole at Site U1530 (Table **T1**). Hole U1530A is located at 34°51.6588′S, 179°3.4572′E at a water depth of 1594.9 m. We used the RCB system to core from the seafloor to 453.1 mbsf and recovered 76.8 m (17%). We encountered optimum downhole conditions throughout coring. After successfully penetrating to target depth, we decided to terminate coring in Hole U1530A to take advantage of the good hole conditions for downhole measurements and fluid sampling. Therefore, we released the bit in the bottom of the hole by deploying the rotary shifting tool.

Our downhole measurement plan for Hole U1530A consisted of running the following tools/tool strings:

- ETBS memory tool,
- 600 mL Kuster FTS tool,
- triple combo tool string (NGR, porosity, and density sondes, including magnetic susceptibility, resistivity, caliper, and logging head temperature),
- Formation MicroScanner (FMS)-sonic tool string, and
- Petrospec spool-in TCMT.

After recording a temperature of 40°C at the bottom of the hole (stationary measurement time of 15 min) with the ETBS memory tool, we lowered the 600 mL Kuster FTS tool on the core line to a depth of ~433 mbsf but did not recover a fluid sample because the valves failed to close completely. We then raised the end of drill string to a logging depth of 67.1 mbsf, lowered the triple combo tool string into the hole, and performed a calibration pass and full logging run from a debris fill at 442 mbsf to the seafloor. This run was followed by two logging passes with the FMS-sonic tool string from 442 mbsf to just below the end of the pipe at 51.8 mbsf. We then lowered the end of the drill string to 416.2 mbsf and obtained a borehole fluid sample with the 600 mL Kuster FTS tool. Finally, the third-party TCMT was deployed on the wireline and, with the temperature-sensitive TCMT data logger kept inside the drill string, the two thermocouple joints were lowered 8 m past the end of the drill pipe and held at 447 mbsf for 10 min. This first test of the newly designed high-temperature TCMT recorded a temperature of 20°C. This test completed our operations at Site U1530. In total, 184.1 h, or 7.7 days, were spent at Site U1530.

Figure F17. Lithostratigraphic summary of Hole U1530A on the caldera wall of the NW Caldera hydrothermal field.

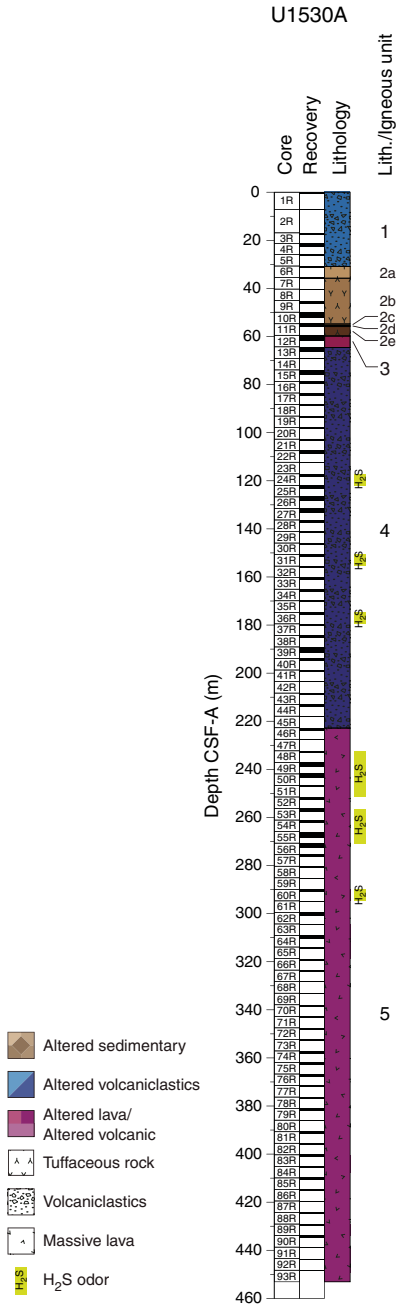


### Principal results

Five igneous units were identified at Site U1530 (Figure **F17**). Igneous Unit 1 (0–26.62 mbsf) consists of clast-supported polymict

Figure F18. Distribution of alteration types and abundance of key minerals, Hole U1530A. Abundance is based on the mineral assemblages determined by XRD and thin section observations.

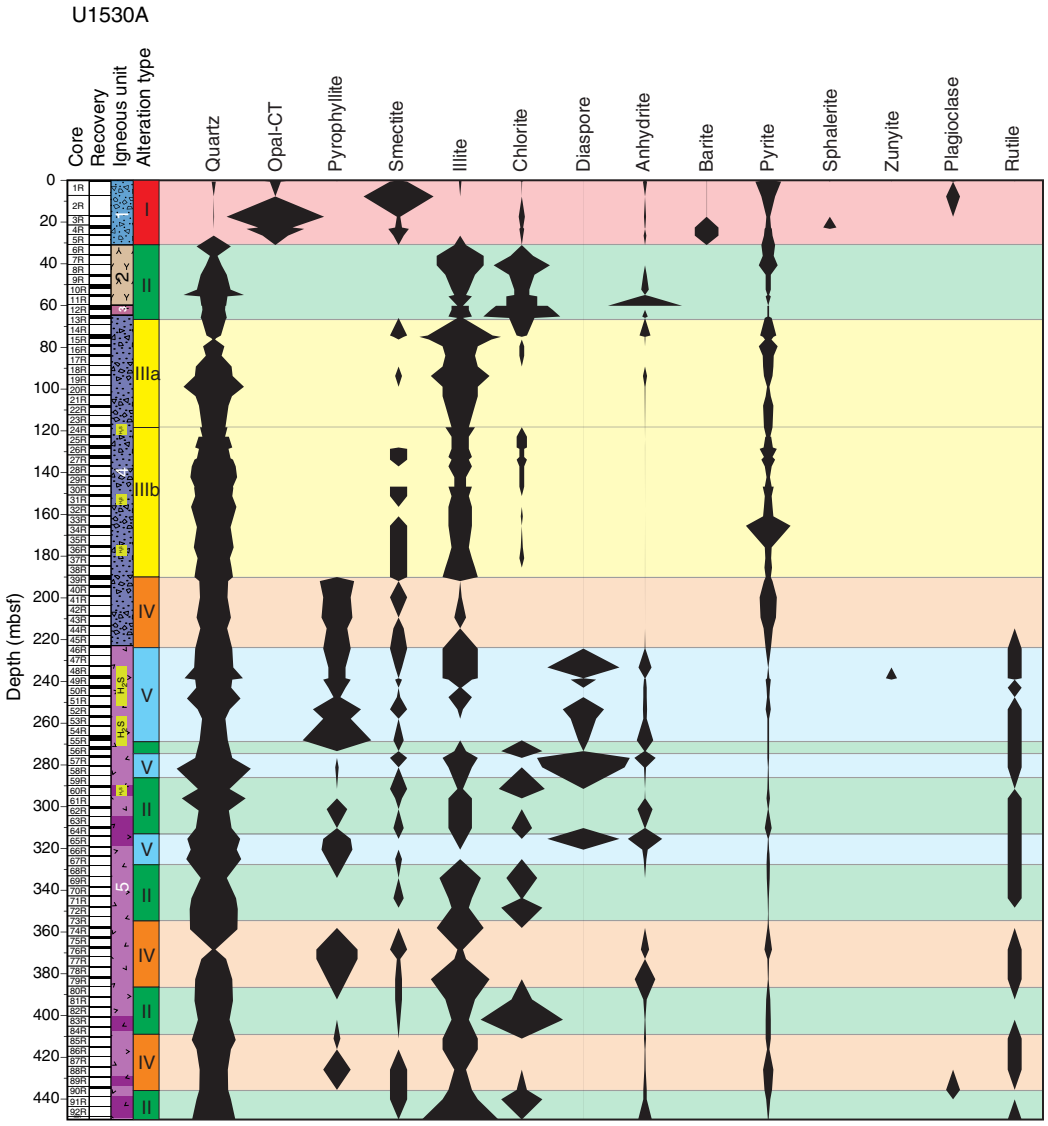


lapillistone with occasional blocks and bombs. Clasts are volcanic in origin and reside in a matrix of altered, smaller volcanic fragments and secondary minerals. Igneous Unit 2 (30.70–59.62 mbsf) consists of a sequence of altered tuffaceous mudstone, siltstone, and sandstone, with one subordinate horizon of polymict lapillistone, and is divided into five subunits (2a–2e) based on color, grain size, and internal structures. Unit 2 displays various sedimentary textures including normal and reverse grading as well as horizontal, wavy, lenticular, and inclined bedding, indicating transport, depositional, and soft-sediment deformation events. Igneous Unit 3 (59.62–64.40 mbsf) consists of altered plagioclase-phyric lava with pseudomorphs after glomerocrystic plagioclase. Igneous Unit 4 (64.40–218.21 mbsf) is a sequence of highly altered volcaniclastic rocks with discernible monomict and polymict lapillistone and monomict lapilli-tuff in the upper half that consists of altered volcanic clasts in a fine-grained, completely altered matrix. Significantly pronounced alteration hinders detailed classification in the lower half of Unit 4. Igneous Unit 5 (222.70–448.68 mbsf) consists of highly altered volcanic rocks with five discrete horizons of less altered plagioclase-phyric lava containing pseudomorphs after glomerocrystic plagioclase.

Despite the pervasive alteration, the volcanic and volcaniclastic rocks retain residual volcanic textures and original compositions of alteration-resistant elements and ratios (Ti, Zr, and Ti/Zr), suggesting that the protolith was a typical Brothers volcano dacite. Similar to the volcaniclastic rocks of Igneous Unit 2 in Hole U1527C, Hole U1530A rocks appear to have the same systematically lower Ti/Zr ratio compared to volcanic rocks at Sites U1528 and U1529. Although this disparity is small compared to the overall range observed in Kermadec arc lavas, it points toward slight genetic variability among the Brothers volcano dacitic magma series.

Five distinct alteration types were identified based on alteration mineral assemblage in core material recovered from Hole U1530A (Figure **F18**). All alteration types occur at various intervals downhole, overprinting each other, and therefore do not correlate with certain depth intervals.

Figure F19. Representative alteration types in hand specimens, Hole U1530A. A. Type I: blue-gray illite-rich clasts crosscut by a network of pyrite-anhydrite-silica veins with a mesh texture. B. Type II: sediment with fine-grained, subhorizontal laminations that are subsequently cut by a vuggy anhydrite vein. C. Subtype IIIa: subrounded to subangular light gray clasts in a gray silicified matrix. D. Subtype IIIb: variably silicified blue-gray clasts exhibiting extensive resorption in a matrix of pyrite intergrown with quartz, with the occasional vug infilled with anhydrite. E. Type IV: homogeneous gray matrix with poorly distinguishable clasts containing patchy pyrophyllite and abundant vugs infilled with quartz and anhydrite. F. Type V: mottled equigranular rock with a clear distinction between light gray quartz-dominated and dark gray diaspore-pyrophyllite–rich areas.

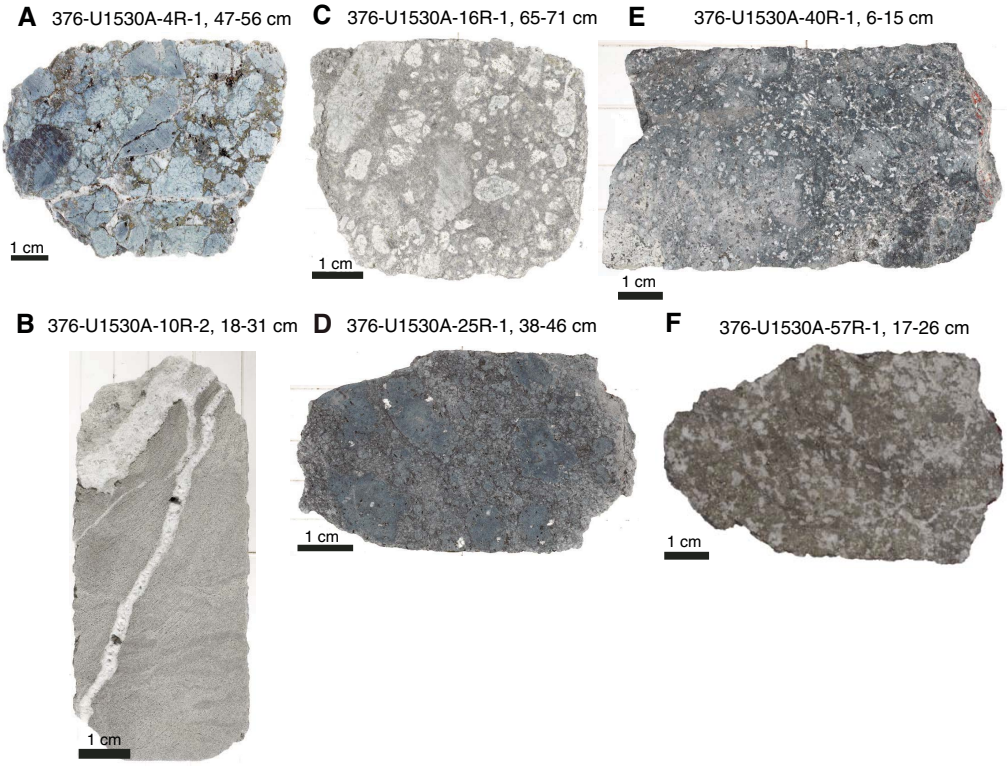


Alteration Type I, classified as highly to intensely altered, has an alteration mineral assemblage of opal, smectite, pyrite, anhydrite, sphalerite, and barite with minor quartz, chlorite, and illite (Figure **F19A**). A network of anhydrite-barite veins with fine- to medium-grained sphalerite cuts blue-gray lapillistone. The clasts are variably altered/silicified, and the contacts between clasts and matrix are distinct. Anhydrite is most abundant in veins and only rarely infills vugs within clasts. In one sample, an acicular mineral, most likely natroalunite, is observed microscopically cutting anhydrite-pyrite-silica veins but was not detected by X-ray diffraction (XRD) analysis.

Alteration Type II, classified as intensely altered, has a characteristic green-gray color and an alteration mineral assemblage of quartz, illite, and chlorite with variable amounts of anhydrite, pyrite, and smectite (Figure **F19B**). Type II is associated with three distinct lithologies throughout the hole: tuffaceous fine-grained sediments, coherent lavas, and pyroclastic rocks. The abundance of individual alteration minerals varies with lithology. For example, pyrite is more abundant in fine-grained sediments compared to pyroclastic rocks. The fine-grained tuffaceous sediment interval (Igneous Unit 2) is frequently cut by coarse-grained vuggy anhydrite veins. The altered lava unit exhibits a vuggy texture, and the vugs are filled with quartz, anhydrite, and minor pyrite. Chlorite and illite are intergrown with microcrystalline quartz, forming a homogeneous matrix. The upper volcaniclastic interval (Igneous Unit 1) is characterized by subangular clasts that are visually distinguishable from matrix material. Clasts are rich in chlorite and illite relative to the silica- and pyrite-rich matrix. Plagioclase is completely pseudomorphed by chlorite, quartz, and occasionally smectite.

Alteration Type III, classified as intensely altered, is characterized by an alteration mineral assemblage of quartz and illite with minor smectite, anhydrite, and chlorite. This alteration type is divided into two subtypes (IIIa and IIIb) based on relative abundances of anhydrite (enriched in Subtype IIIa) and chlorite (enriched in Subtype IIIb). Subtype IIIa is white-gray and consists of well-defined pyroclastic texture with soft illite-rich clasts within a silica- and pyrite-rich matrix (Figure **F19C**). Subtype IIIb is blue-gray, and both matrix and clasts are intensely silicified (Figure **F19D**). Pyrite occurs as a minor phase disseminated throughout. Fe oxyhydroxide is likely derived from pyrite oxidization. Magnetite is an accessory phase and is frequently partially resorbed and overprinted by pyrite.

Alteration Type IV, classified as intensely altered, is light gray and has a mineral assemblage of pyrophyllite, quartz, illite, and smectite with minor pyrite and rutile (Figure **F19E**). Clasts are poorly defined and strongly resorbed. Pyrophyllite is patchy and intergrown with illite and disseminated fine-grained anhydrite and likely represents the core of relict clasts. Quartz is intergrown with illite and forms discrete veins associated with subhedral pyrite. Common leucoxene and minor rutile form <0.1 mm grains and are variably overprinted by pyrite.

Alteration Type V is buff colored and occurs as two distinct textures: fine-grained homogeneous material and coarse-grained equigranular material with a mottled texture (Figure **F19F**). Both textures exhibit the same alteration mineral assemblage of diaspore,

Figure F20. Salinity (NaCl equivalent wt%) vs. homogenization temperature and corresponding enthalpy of NaCl-$H_2O$ (Bischoff and Rosenbauer, 1985) for fluid inclusions from anhydrite, Site U1530. The critical line divides the diagram into the supercritical and subcritical zones. NaCl saturation curve calculated from Driesner and Heinrich (2007); NaCl vapor conjugate curve calculated from Bischoff (1991). Phase separation (boiling) curves calculated for seawater and for 41 wt% NaCl equivalent hypersaline brine (bc1). Salinities measured near the seawater line may be due to condensation from a supercritical NaCl vapor. Hypersaline brine salinities above the NaCl saturation curve may be caused by boiling (bc1) or a NaCl brine with additional major cations such as K (line NK).

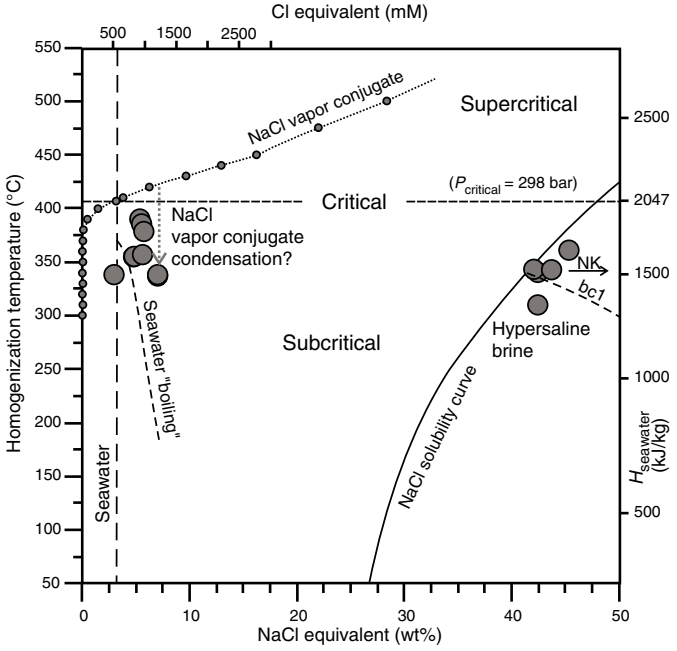


quartz, pyrophyllite, smectite, and rutile with minor illite, pyrite, and anhydrite. Fe oxyhydroxide staining is well developed throughout this alteration type, and pyrite is absent in some samples. Vugs are abundant and commonly infilled with chalcedony and anhydrite; the latter fills the core of the vugs. Anhydrite occurs in two distinct generations: coarse euhedral grains that infill vugs and veins and a fine-grained subhedral to euhedral form intergrown within the matrix. Rutile occurs in traces, mantled or overprinted by pyrite.

Unlike veins in Hole U1528D, most veins in Hole U1530A are sealed with anhydrite + sulfides + quartz, and only a few vugs are partly filled by drusy quartz or anhydrite that may record the latest fluid compositions and temperatures. All fluid inclusions are two-phase and homogenize to the liquid phase at 209° to 390°C, except for one (406 mbsf) that exhibits critical-point behavior at 345°C. The highest homogenization temperatures are measured in Alteration Types V (key minerals are pyrophyllite + diaspore) and II (key minerals are illite + chlorite). By contrast, the lowest median temperature of 255°C was determined at 291 mbsf. The salinities of fluid inclusions plot into two separate regions: at or near seawater compositions and as a hypersaline brine at or along the NaCl saturation curve (Figure **F20**). Only Alteration Types II and V can be associated with hypersaline brines. The fluid inclusion data are consistent with two different fluids being responsible for the alteration assemblages: a pervasive fluid of modified seawater composition that has been heated to about 390°C and a hypersaline brine heated to 288°–390°C (Figure **F20**).

Structures in Hole U1530A consist of volcanic fabrics, alteration veins, fractures, and sedimentary boundaries. Sedimentary boundaries, defined by changes in grain size and/or texture, are all subhorizontal (<10°). Volcanic fabrics are in two forms: within volcanic clasts or within coherent lava. In both forms, the fabric is defined by vesicles and plagioclase microlites. Volcanic fabrics within clasts can be weak to strong but do not share a common orientation across clasts. This type of fabric is observed in the uppermost half of Hole U1530A in lapilli-tuffs defining Igneous Units 1 and 4. Moderate to strong volcanic fabrics that occur over decimeters define Igneous Units 3 and 5, which consist of lavas. Volcanic fabrics within the lavas tend to be moderate to steep, with dips >45°.

Alteration veins occur throughout the hole and are typically filled with anhydrite, silica, and/or pyrite. Vein density is variable downhole, and the highest density relates to the presence of network veins, typically filled with pyrite or silica. The largest abundance in network veins is at the very top of the hole, from 0 to 25 mbsf. Discrete veins are most abundant at ~70 and ~270 mbsf. These depths also correspond to a large range in vein dip (0°–90°), an increase in vein thickness, and at ~270 mbsf a deviation in borehole temperature. These depth intervals are also related to changes in igneous rock type between sediments and lavas above lapilli-tuff at ~70 mbsf and a change from lapilli-tuff to lava at ~270 mbsf. The presence of sedimentary and volcanic rocks, the large range in vein dip and thickness, and a deviation in borehole temperature may indicate the presence of lateral flow zones related to permeability contrasts. Fractures are less abundant compared with veins but are more common than at any other site. Fractures have a large range in dip and are more frequent at ~55 and ~255 mbsf, which is coincident with zones of more abundant veins. Slickenlines were identified from ~190 to 290 mbsf and typically have steep rakes and a normal sense of shear.

All hard rock samples from Site U1530 show various degrees of hydrothermal alteration, as confirmed by petrographic descriptions and analysis via XRD and ICP-AES/portable X-ray fluorescence (pXRF). Despite pervasive alteration, the volcanic and volcaniclastic rocks have retained original chemical compositions of alteration-resistant elements and ratios (Ti, Zr, and Ti/Zr) that suggest the protolith was a typical Brothers volcano dacite. Relative to Site U1528 and U1529 rocks that have a Ti/Zr value of ~36, Hole U1530A and U1527C volcanic and volcaniclastic rocks appear to share the slightly but systematically lower Ti/Zr value of ~27. Although this disparity is smaller than the overall range observed in Kermadec arc lava (Ti/Zr ≤ 220), it points to slight genetic variability among the Brothers volcano dacitic magma series. For a large range of alteration-sensitive elements, the recovered rocks display strong geochemical changes and major loss of Mn, Ca, and Na (Figure **F21**). The observed downhole variations of major oxides and trace elements are much more pronounced at Site U1530 than at Site U1527, including the extensive loss of $Na_2O$ relative to unaltered dacites recovered at Sites U1527 and U1529. Other alkali elements, such as potassium ($K_2O$) and the alkaline-earth metals (Mg, Ca, Sr, and Ba), show both depletions and enrichments relative to fresh dacites. The strongest geochemical shifts in Hole U1530A occur at 189–191 mbsf, where a decrease in $K_2O$, Ba, Y, and Cu concentrations corresponds to the transition from Alteration Type III to IV and the disappearance of illite and first appearance of pyrophyllite. Alteration Types IV and V in Igneous Unit 5 form two important end-members and display the strongest depletions in Mg, Ba, Sr, Fe, Cu, and Zn. The reverse pattern is seen in Alteration Type I in Igneous Unit 1, suggesting that some of the loss of elements observed at

Figure F21. Variations in major element oxides in altered volcaniclastic rocks and lavas, Hole U1530A. Average values for fresh dacites recovered from Hole U1527A and at Site U1529 are shown with dashed vertical lines representing 2σ from average values.

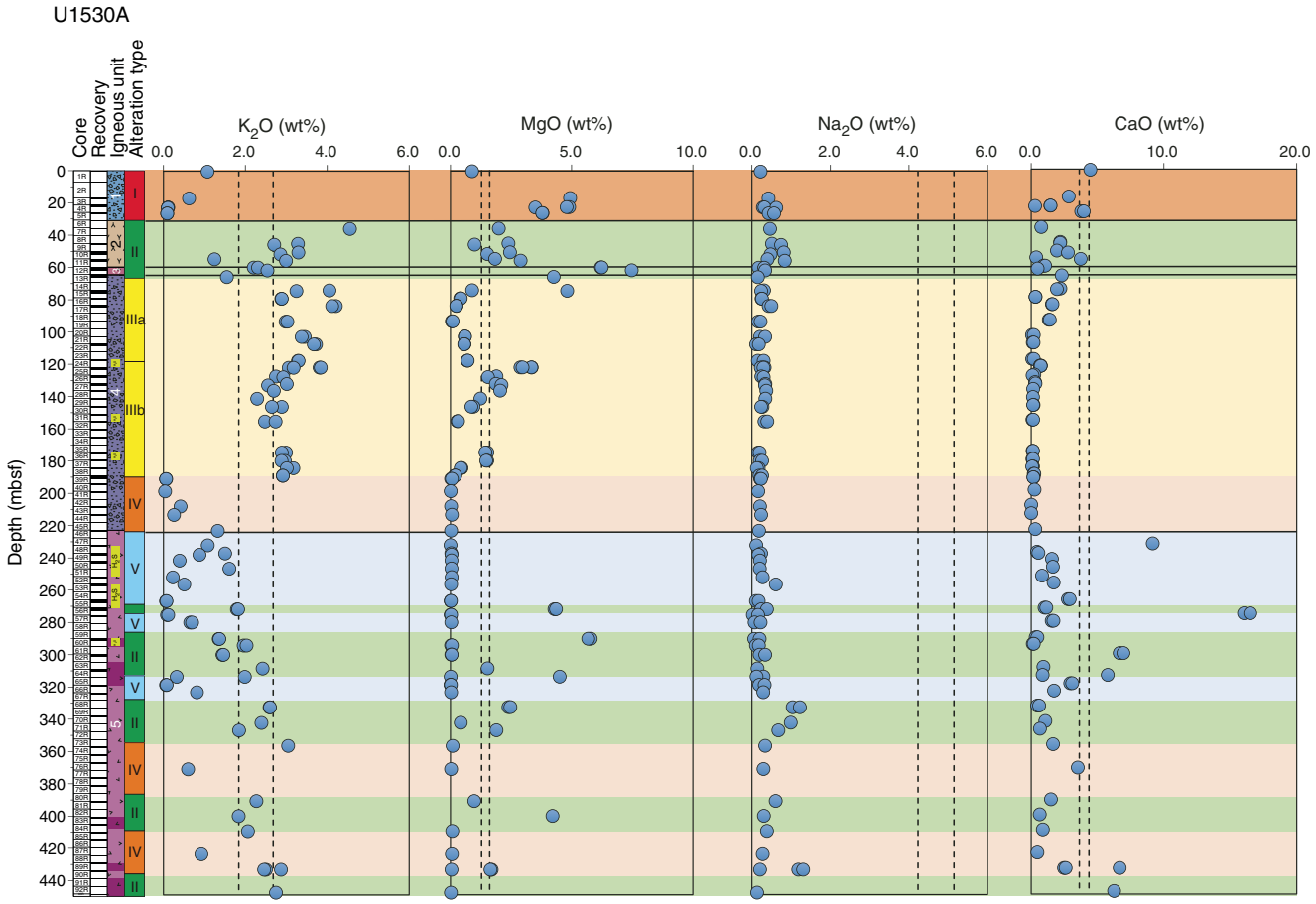


the bottom of the hole may partially be balanced by a gain of these elements in the upper part of the hole. Depletions in CaO are associated with higher Sr concentrations and the identification of anhydrite by XRD, suggesting that the abundance of CaO is mainly controlled by the occurrence of anhydrite. Principally hosted in barite, Ba at Site U1530 ranges from trace levels of about 20 µg/g in Alteration Types IV and V to very high abundances of about 3 wt% in Alteration Type I. A pronounced correlation was observed between total S and Fe concentrations throughout Hole U1530A, suggesting that pyrite represents the primary form of S in the rock (predominantly in Igneous Units 1, 2, and 4). Significant enrichments in Zn (≤5.2 wt%), Cu (≤1760 ppm), As (≤660 ppm), Pb (≤100 ppm), and Mo (≤560 ppm) were also recorded in pyrite-rich intervals, consistent with high-temperature hydrothermal fluid contributions.

TC content in the majority of Hole U1530A samples are <200 µg/g and are lower overall than TC content at Sites U1527–U1529. An average total sulfur content at Site U1530 of 5.1 wt% is similar to the 5.9 wt% average at Site U1528. In contrast to Site U1528, total sulfur content decreases with depth from ~11 to ~3.5 wt%, on average.

Pore space dissolved gases, including $H_2$, CO, $CH_4$, $C_2H_6$, $\Sigma CO_2$, and acid-volatile S, were analyzed from several intervals of the recovered cores in Hole U1530A. As reported at Sites U1527–U1529, pore space dissolved $C_2H_6$ concentrations were below detection limit (<0.03 µmol/L) for all depths in Hole U1530A. Five intervals with elevated $H_2$, $CH_4$, $\Sigma CO_2$, and acid-volatile sulfide (AVS) concentrations were detected. Maximum pore fluid AVS and $\Sigma CO_2$ concentrations of 1.6 and 37 mM, respectively, are similar to those previously determined by de Ronde et al. (2011) for actively venting chimneys of the NW Caldera vent field and may originate from fluids rich in magmatic volatiles.

A fluid sample was collected with the 600 mL Kuster FTS tool at 435 mbsf. The in situ fluid temperature was estimated to be <38°C based on downhole temperature logging. The borehole fluid sample is slightly acidic relative to seawater (pH 6.8) and is characterized by the same major and minor species composition (i.e., dissolved Na, K, Ca, Sr, Mg, Cl, Br, and $\Sigma SO_4$) as drilling fluid (surface seawater) within analytical error. Dissolved $\Sigma H_2S$ concentration is below detection limit. The concentrations of several metal species are highly elevated above seawater values and are likely derived from contamination by the steel bit and drill string or the 600 mL Kuster FTS tool itself.

The NRM of 81 archive halves from Hole U1530A was measured using the cryogenic superconducting rock magnetometer (SRM). The overprint magnetization from drilling and coring was reduced by using the in-line AF demagnetizer. Detailed measurements of anisotropy of magnetic susceptibility (AMS), AF and thermal demagnetization, and IRM experiments on 65 discrete oriented samples were also conducted (four from Igneous Unit 1, five from Igneous Unit 2, two from Igneous Unit 3, twenty-four from Igneous Unit 4, and thirty from Igneous Unit 5). Magnetic directions for discrete samples show relatively shallow inclinations compared with

Sites U1527 and U1528. In particular, three samples from Igneous Unit 2 (Core 376-U1530A-10R to Core 11R; 50–55 mbsf) show consistent positive inclinations, confirmed by corresponding pieces measured in the cryogenic magnetometer. The NRM intensities and magnetic susceptibilities also highlight relative differences between the various igneous units. For example, Igneous Unit 1 is characterized by low NRM intensities, low coercivities, and erratic thermal demagnetization curves. Igneous Units 2 and 4 are characterized by very low NRM intensities with complex AF and thermal demagnetization curves but larger coercivities. Igneous Units 3 and 5 have low NRM intensities, low-to-medium magnetic coercivities, and relatively simple AF and thermal demagnetization curves with a minor overprint from drilling. Igneous Units 1, 2, and 4 also show increases of NRM intensity after heating to temperatures >400°C, suggesting irreversible transformation of the original magnetic minerals during heating.

Variations of physical properties at Site U1530 show good correlations with defined igneous units and subunits but correlate less well with transitions in alteration types. Igneous Unit 1, which corresponds to Alteration Type I, contains the peak values for magnetic susceptibility and NGR at the site. NGR peaks are also recorded by downhole measurements with the Hostile Environment Natural Gamma Ray Sonde (HNGS) and are an order of magnitude higher than those recorded at the other Brothers volcano drill sites, which is attributed to radioactive U-series isotopes in the sulfide and barite veins observed at this depth.

Transitions between and within igneous units and subunits are clearly defined by variations in bulk density, porosity, and *P*-wave velocity. These data do not show strong correlation with structural features such as fractures or alteration veins. Observed variations in magnetic susceptibility and thermal conductivity do not correspond clearly to the observed abundance or distribution of particular minerals, but a large increase in magnetic susceptibility from Igneous Unit 4 to 5 is evident.

Overall, physical property data define two intervals of markedly different characteristics: ~30 to ~35 mbsf in Igneous Unit 2 and ~75 to ~85 mbsf in Igneous Unit 4. These intervals are characterized by high grain density, low bulk density, and high porosity. They also correspond to increased concentrations of $Fe_2O_3$, S, trace metals, and metalloids and are located directly beneath intervals characterized by increased fracture density and wide ranges in alteration vein dip angles. These intervals may therefore be important for understanding the past fluid–rock interactions and flow pathways of the hydrothermal system at Site U1530.

Multiple borehole temperature measurements obtained over the downhole logging period indicated that the hole had warmed from ~35° to 94°C at ~430 mbsf during the first 5 h after stopping circulation and then had cooled to 37°C during the subsequent 10 h. The temperature profile shows a gradual increase in temperature with depth, indicative of a largely conductive-dominated regime in the borehole, and also displays a concave-upward shape suggestive of recharge into the formation. Thermal anomalies in the temperature profiles observed between 255 and 295 mbsf may indicate a permeable flow zone. This interval is also characterized by the highest number of veins with a large range in vein dip and a higher abundance of fractures, suggesting structural control for this permeable zone. Downhole caliper measurements showed an overall comparatively large borehole diameter partially exceeding the measurable 43.2 cm (17 inches), with a minimum of 24.0 cm (9.5 inches) and a median of 41.1 cm (16.2 inches). Downhole NGR measurements reveal high U-series isotopes between 23 and 35 mbsf, correlating well with high values measured on the recovered core and most likely related to barite identified by XRD analysis. High potassium concentration corresponds to Alteration Types II and III, both of which contain abundant illite. Downhole density and porosity measurements are in good agreement with discrete core measurements. The depth interval between 70 and 85 mbsf in Igneous Unit 4 and Subtype IIIa alteration has low bulk density and resistivity and high porosity from both discrete and downhole measurements.

In total, 18 whole-round samples (5–11 cm long) were collected from Hole U1530A for microbiological analysis (Table **T2**). Samples were processed for shore-based DNA and RNA analyses, cell and viral counting, and viral and microbial activity measurements. PFMD was used for contamination testing and was usually detected on the outside of uncleaned cores and, on rare occasions, was above detection limit on the cleaned outside of cores. However, concentrations of PFMD in drilling fluid samples were much lower than the expected 500 ppb values. Based on the results, the decision was made to increase the PFMD tracer pumping rate by a factor of 10 at the next drill site (U1531) and to collect drilling fluid from every core.

## Site U1531

### Background and objectives

Site U1531 (proposed alternate Site LC-1A) is located on the saddle between the Lower and Upper Cones of Brothers volcano (Figure **F6**). This site likely sits between the margins of the upflow zones of both the Upper and Lower Cones because there is no detectable low crustal magnetization in this area. The Lower Cone hydrothermal vent field includes vents that discharge the most Fe- and Mg-rich fluids sampled at Brothers volcano to date, although there is no evidence for venting at the saddle. The main objective of Site U1531 was to drill and core to ~300 mbsf to sample the various volcanic cycles that compose the Lower Cone as well as to intersect the upflow zone of metal-rich fluids.

### Operations

We implemented operations in five holes at Site U1531 (Table **T1**). Holes U1531A, U1531B, and U1531E were drilled on the saddle stretching between the Lower and Upper Cone of Brothers volcano. Holes U1531C and U1531D were established on the summit of the Lower Cone. Hole U1531A is located at 34°52.7767′S, 179°4.2241′E at a water depth of 1354.9 m. In this hole, we conducted RCB coring from the seafloor to 15 mbsf, with poor recovery of 1.0 m (7%). Further advancement was impossible because of extremely poor hole conditions that led to a stuck drill string several times. In Hole U1531B, located at 34°52.7721′S, 179°4.2111′E at a water depth of 1351.9 m, RCB coring penetrated from the seafloor to 26 mbsf and recovered 4.0 m (15%). However, poor hole conditions in blocky/fragmented lava deposits prevented us from further deepening the hole. We offset the vessel ~110 m northeastward to the summit of the Lower Cone to Hole U1531C at 34°52.7239′S, 179°4.2586′E at a water depth of 1306.9 m. Here, we RCB cored from the seafloor to 28.4 mbsf and recovered 2.3 m (8%), with tight hole conditions throughout coring. We thus abandoned Hole U1531C at 28.4 mbsf.

We then decided to deploy a reentry system with a short 16 m long casing string to establish a stable hole for reaching deeper coring and logging objectives. We drilled in casing in Hole U1531D at 34°52.7228′S, 179°4.2606′E at a water depth of 1306.9 m at the summit of the Lower Cone. After the pilot bit drilled to the target depth of 19 mbsf, we released the reentry system from the drilling assembly (mud motor, underreamer, and drill bit), but we were unable to

pull the drilling assembly clear of the casing string because the underreamer arms did not completely retract. After several hours of attempting to free the reentry system, we started pulling the drill string and attached reentry system out of the hole and back to the vessel. While we were retrieving the casing reentry system assembly, it unfortunately dropped off in sight of the moonpool, with our position above the bottom part of Lower Cone slope in its transition to the surrounding southeastern caldera floor.

We then moved back to the saddle between the Lower and Upper Cone and made up another drilling assembly to drill-in 16 m of casing in Hole U1531E located at 34°52.7591′S, 179°4.2344′E at a water depth of 1350.4 m. We drilled-in the casing to 17.9 mbsf. We then conducted another test of the CDEX TDCS and washed down (drilled without coring) to 17.9 mbsf to start coring in Hole U1531E. We could not advance any deeper because the TDCS core barrel got stuck in the BHA and could not be retrieved. After the TDCS test, we cored with the RCB system from 17.9 to 39.6 mbsf and recovered only 0.8 m (4%). At this point, the blower motor in the top drive failed. We decided not to repair it at this time because of our remaining scientific priorities and the approaching end of the expedition. Our final operation at Site U1531 consisted of a downhole temperature measurement with the ETBS memory tool. It recorded a maximum temperature of ~5°C at 20 mbsf. In total, 264.3 h, or 11.0 days, were spent at Site U1531.

### Principal results

At Site U1531, one igneous unit is observed in Holes U1531A (0–1.14 mbsf), U1531B (0–21.97 mbsf), U1531C (0–23.75 mbsf), and U1531E (17.90–34.95 mbsf) and in several ghost cores from Hole U1531E. Igneous Unit 1 consists of unaltered to slightly altered plagioclase-pyroxene-phyric dacite lava intercalated with unconsolidated ash, ash with lapilli, and lapilli tephra with ash. The moderately to highly vesicular dacite lava contain glomerocrysts and phenocrysts of plagioclase, orthopyroxene and clinopyroxene, and Fe-Ti oxides in cryptocrystalline and hypocrystalline groundmass. Volcaniclastic material is mainly composed of unaltered dacite clasts, crystals, and subordinate lithic components. The composition of the dacite lava and pyroclastic rocks at Site U1531 is typical for those of the youngest dacitic magmas erupted at Brothers volcano.

Based on the alteration mineral assemblage, one alteration type was identified at Site U1531. Alteration Type I, classified as slightly altered, has an alteration mineral assemblage of smectite, Fe oxyhydroxide, zeolite, pyrite, and rarely native S. Alteration occurs as infilling and lining of vesicles as well as smectite replacing the glassy matrix.

The main structures at Site U1531 include volcanic fabrics and fractures. Volcanic fabrics ranging from weak to strong were observed in all holes. Only three depth intervals across Site U1531 are structurally isotropic. Fabrics are defined by elongated vesicles, plagioclase microlites, and subordinate plagioclase phenocrysts and glomerocrysts. Vesicles have aspect ratios between 5 and 15. Hole U1531C is the only hole where fabric orientation was measured. Fabric dips range from moderate to steep. A few pieces in Hole U1531C have lineations defined by vesicles; all plunges are subparallel to the dip. Several core pieces from all holes have microfractures delineated by the growth of halite and gypsum after pieces were cut and dried. Discrete fractures are best preserved in Hole U1531C. Fractures range from shallow to steep and are typically marked by secondary minerals such as native sulfur or Fe oxyhydroxide.

Unaltered to slightly altered lavas and tephra from Igneous Unit 1 represent typical dacites, with 62.3–65.0 wt% $SiO_2$ and $Na_2O$ + $K_2O$ content ranging from 6.5 to 6.9 wt%. The dacites are essentially similar in major and trace element composition to fresh dacites at Site U1529 and Hole U1527A (Igneous Unit 1) and confirm the low compositional range previously reported for dacites at Brothers volcano. TC and total sulfur contents are generally low (<250 and <300 µg/g, respectively) except in one sample with TC ≈ 1900 µg/g. Low total sulfur is consistent with previously reported data for dacitic glass at Brothers volcano, suggesting minimal influence of magmatic volatile input in the selected samples. However, the detection of relatively high concentrations of $H_2$ and AVS in some intervals is consistent with discharging magmatic gases through the volcanic pile.

Only three core sections recovered from Site U1531 (i.e., Hole U1531C) had oriented pieces that could be measured in the cryogenic SRM. In addition, we selected five discrete samples from the working halves for detailed measurements of AMS, AF and thermal demagnetization, and IRM experiments. As expected from fresh dacites, NRM intensities are large. Magnetic directions from these samples have inclinations of approximately −60°, suggesting a very young age for the primary magnetization component. The shape of the thermal demagnetization curve indicates that these samples contain pure magnetite and titanomagnetite with variable Ti content.

Physical property measurements made on limited fragmented core samples recovered from Holes U1531A–U1531C and U1531E are consistent with the range of expected values for fresh dacite lava and tephra and are similar to those for fresh volcaniclastic material from Igneous Unit 1 at corresponding Sites U1527–U1529. No clear difference in physical properties is evident between material recovered from the summit of the Lower Cone and material recovered from the saddle, although interpretation is significantly limited by the low recovery, fragmented nature of the core, and limited number of oriented pieces.

The ETBS memory tool was deployed in Hole U1531E after ~24 h without circulation. It recorded a maximum temperature of 5.2°C at 20 mbsf, which is similar to the bottom seawater temperature.

One whole-round sample of moderately vesicular dacite lava was collected from Hole U1531C for microbiological analysis (Table **T2**). Sample aliquots were taken and preserved for shore-based DNA and RNA analyses, as well as prokaryotic and viral counting and activity measurements.

## Preliminary scientific assessment

Expedition 376 was designed to provide the missing link (i.e., the third dimension) in our understanding of hydrothermal activity and mineral deposit formation at submarine arc volcanoes and the relationship between the discharge of magmatic fluids and the deep biosphere. The drill sites targeted areas considered to be hydrothermal upflow zones of geochemically distinct fluids that are variably affected by magmatic volatile input, thus allowing us to directly address the consequences of magma degassing for metal transport to the seafloor and its effect on the functioning of microbial communities.

Expedition 376 completed five sites: two (Sites U1527 and U1530) within the NW Caldera seawater-dominated hydrothermal field, two (Sites U1528 and U1531) within the Upper and Lower Cone magmatic fluid–influenced hydrothermal fields, and one (Site U1529) in an area of low crustal magnetization that delineates the W Caldera upflow zone. Although three of these sites were original

primary sites and one (Site U1531) an original alternate site, Site U1530 was added during the expedition. This addition was needed because we encountered much thicker than expected loose, unconsolidated volcanic gravels, sands, and ash-like material that caused significant drilling difficulties early in the expedition, particularly for Site U1529 on the caldera floor; Hole U1529B collapsed after only ~34 m of penetration. Hence, we sought and obtained approval to move an alternate caldera floor site to a new location on a bench on the NW Caldera wall (Site U1530) to minimize the likelihood of an overburden of unconsolidated volcaniclastic material.

Expedition 376 used rotary coring for most sites, but it also tested a prototype TDCS developed by Japan Agency for Marine-Earth Science and Technology (JAMSTEC) in Holes U1528C and U1531E. Drilling was extremely successful, coring 1244 m and recovering 222.4 m of core. This is almost four times the recovery achieved during ODP Leg 158 (TAG hydrothermal field, Mid-Atlantic Ridge; Herzig, Humphris, Miller, and Zierenberg, 1998) and almost three times that of Ocean Drilling Program (ODP) Leg 193 (PACMANUS hydrothermal field, Eastern Manus Basin; Barriga, Binns, Miller, and Herzig, 2007), which represent the two previous endeavors with volcanic rock–hosted hydrothermal systems as drilling targets. Important to the success of Expedition 376 was the use of drill-in casing, which provided stability in the volcaniclastic deposits encountered in the upper part of some holes. Overall, recovery averaged 18% for Expedition 376 (cf. 13% for Leg 158 and 11% for Leg 193) and varied between 1% (Hole U1527A) and 29% (Hole U1528D), depending on the hole conditions and lithologies encountered. Downhole measurements and borehole fluid sampling were conducted in Holes U1528D, U1530A, and U1531E. Given the low and variable recovery, the downhole logs from Sites U1528 and U1530 will be extremely helpful postexpedition in the interpretation of the rock record.

We expect that integration of the shipboard data with postexpedition shore-based analyses will result in significant progress toward addressing all four of the primary scientific objectives outlined in the Expedition 376 *Scientific Prospectus* (de Ronde et al., 2017):

1. *Characterize the subvolcano, magma chamber–derived volatile phase to test model-based predictions that this is either a single-phase gas or two-phase brine-vapor.*

Hole U1528D penetrated 359.3 m through the center of the Upper Cone, beginning at the floor of a pit crater at its summit. Much of the core recovered from this hole smelled strongly of $H_2S$, and a mineral assemblage of illite + natroalunite + pyrophyllite + quartz + opal + pyrite attests to acid-sulfate fluids derived from the disproportionation of magmatic gases, such as $SO_2$. Headspace gas analyses confirm relatively high levels of AVS (as much as 20 mmol/L near the bottom of the hole) and $\Sigma CO_2$ (as much as 182 mmol/L). The effects of strong acid on the host rock are also reflected in the geochemical data, which indicate extreme depletion of major elements, such as MgO, $K_2O$, and $Na_2O$. Furthermore, very acid (pH as low as 1.8), relatively hot (≤247°C) fluids collected by the 600 mL Kuster FTS tool at 160, 279, and 313 mbsf have compositions that are indicative of significant magmatic gas input. In addition, preliminary fluid inclusion results provide evidence for two dominant fluids having transgressed the Upper Cone: a hot (≤340°C) hydrothermal fluid of modified-seawater origin that appears to have undergone phase separation and a hot (≤360°C) hypersaline brine that may be transporting metals, given the observation of sulfide daughter crystals (together with halite) in some of the inclusions. The highest fluid inclusion homogenization temperatures are coincident with a high-temperature acidic alteration mineral assemblage of natroalunite + pyrophyllite + opal, indicating temperatures of ≥230°C (e.g., Reyes, 1990). These results clearly show brine-vapor conditions occurring within the Upper Cone site at Brothers volcano.

Hole U1531E penetrated 39.6 m into the southwest flank of the Lower Cone immediately east of the saddle between the lower flanks of the Upper and Lower Cones. Cores recovered from this hole are largely fresh lavas with only incipient low-temperature alteration, although native S coating the walls of small fractures indicates limited interaction with magmatic volatiles and/or hydrothermal fluids. However, the observation of extensive diffuse venting of gassy, very acidic fluids emanating from and surrounding the summit of the Lower Cone (de Ronde et al., 2011) implies that magmatic degassing must be restricted to narrow upflow zones.

Further shore-based studies, including additional analyses of the borehole fluids and more extensive fluid inclusion studies, will help constrain the characteristics of the fluids within the Upper Cone hydrothermal system and allow us to test models of the subsurface hydrologic regimes at Brothers volcano.

2. *Explore the subseafloor distribution of base and precious metals and metalloids and the reactions that have taken place along pathways to the seafloor.*

Holes U1527C and U1530A are located in different parts of the NW Caldera hydrothermal vent field. The former is on the western margin of the field atop the caldera rim, and the latter is on the caldera wall. Hole U1527C was drilled to 238 mbsf and penetrated variably altered volcaniclastic rocks and coherent lavas of dacitic composition. The upper 185 m of Hole U1527C are dominated by a mineral assemblage of goethite + opal + mordenite, which is indicative of relatively low temperature (<150°C) alteration. This assemblage is replaced downhole by chlorite + quartz + illite ± smectite, and the lower parts of the hole are characterized by an assemblage dominated by quartz + chlorite + pyrite ± illite. These assemblages indicate alteration temperatures >230°C. Pyrite is the predominant sulfide phase in Hole U1527C and is disseminated mainly in the deeper chlorite + illite–rich part of the core.

Hole U1530A was established proximal to a fault that exposes a stockwork zone, where several centimeter-thick, metal-rich veins form an anastomosing network within the altered host rock. Hole U1530A was drilled to 453 mbsf through a sequence of altered volcaniclastics with intercalated coherent lavas and an interval of altered tuffaceous sediments. The upper ~30 m of core have a mineral assemblage of opal + smectite + chlorite + pyrite + barite + sphalerite, which is indicative of alteration temperatures of 100°–250°C. The occurrence of sphalerite and pyrite in close proximity to the sulfate minerals along with the presence of a dense network of veins averaging 0.2 cm in thickness and enrichment in metals and metalloids (Zn, As, Cu, Mo, Se, and Pb) is consistent with the proximity of the hole to the exposed stockwork zone.

This assemblage is replaced downhole by quartz + illite + chlorite + anhydrite, which points to alteration temperatures <275°C. More acid (pH < 4) and hotter (250°–300°C) fluids are implied even further downhole with the appearance of pyrophyllite deeper than ~190 mbsf followed by a final assemblage of diaspore + quartz + pyrophyllite + rutile ± zunyite deeper than ~225 mbsf. Two-phase fluid inclusions (with and without daughter halite crystals) associated with the pyrophyllite- and diaspore-rich alteration assemblages have homogenization temperatures of ~350°–390°C. Other inclusions are complex and contain various daughter minerals, including

halite, sulfates, and other anisotropic minerals, with homogenization temperatures >320°C. Combined, the fluid inclusions are indicative of hypersaline brines like those seen in fluid inclusions at Upper Cone Site U1528. Pyrite is the main proxy for metals in the borehole and is distributed throughout the hole, although more abundant in the chlorite + illite–rich zones. The loss of K, Ba, Y, and Cu deeper than ~190 mbsf and an increase in the magnitude of depletion deeper than ~225 mbsf, corresponding to the appearance of pyrophyllite and diaspore, are also consistent with a downhole decrease in pH and increase in temperature (above ~250°C) of fluid–rock reaction. Later incursion and mixing of seawater and hydrothermal fluid that overprints earlier mineral assemblages resulting from reaction with more acidic fluids is reflected in the increased abundances of smectite, chlorite, and anhydrite in a later alteration event.

The large variations observed in the alteration mineral assemblages encountered at Sites U1527, U1528, and U1530 clearly attest to complex but distinct paragenetic sequences at both the NW Caldera and the Upper Cone hydrothermal fields. Interestingly, it appears that the currently seawater-dominated NW Caldera hydrothermal field may have undergone an earlier phase of reactions with acid-sulfate fluids, resulting in alteration assemblages resembling those observed in the Upper Cone. Further mineralogical, geochemical, and fluid inclusion shore-based studies will elucidate the reactions that take place along pathways to the seafloor and the distribution, transport, and fate of metals and metalloids within the hydrothermal systems of Brothers volcano.

3. *Quantify the mechanisms and extent of fluid-rock interaction, the consequences for mass transfer of metals and metalloids into the ocean, and the role of magmatically derived carbon and sulfur species in mediating these fluxes.*

Fluid-rock reactions at Sites U1527, U1528, and U1530 have occurred under a range of conditions (i.e., temperature, pH, Eh, etc.), and hence quantifying mass transfer of elements into the ocean is difficult, particularly given the heterogeneous lithologies encountered at all sites. The mineral assemblage of quartz + illite + chlorite + anhydrite ± smectite in Holes U1527C and U1530A in the NW Caldera hydrothermal vent field clearly points to a complex exchange between a hydrothermal fluid of modified-seawater composition and the dacitic protolith. This is indicated by Mg and S enrichment as well as both depletion and enrichment in K and Rb, respectively, in addition to relatively subtle changes in other major elements (normalized to the composition of unaltered dacitic lava from Site U1527). These element exchanges are distinct from those observed in the mineral assemblage that is indicative of interaction with hot acidic fluids (i.e., denoted by the assemblage of pyrophyllite + diaspore + quartz + illite ± rutile) seen deeper in Hole U1530A, which shows strong depletions in K, Mg, Ca, Na, and Fe contents.

In contrast, at the Upper Cone site, alteration and elemental exchange are affected by magmatic volatile–driven reactions. Magmatic gases (high concentrations of $H_2$, $\Sigma CO_2$, and AVS were measured in headspace gas analyses) cool, condense, undergo disproportionation reactions involving $SO_2$, $\Sigma H_2S$, and $\Sigma SO_4$, and mix with seawater as they ascend toward the seafloor. The resulting acidic hydrothermal fluids strongly leach the rocks of the Upper Cone. The leaching leads to depletion of many major elements, including Mg, K, Na, Fe, Ca, and Mn, and enrichment in S (note that the loss of Fe may be related to interaction with a later-stage, sulfate-rich fluid). Fluid inclusion data from Hole U1528D suggest that most metals are likely still at depth, given the highly saline (33 wt% equiv. NaCl) brines, with noticeable sulfide daughter minerals included. Active venting at the Upper and Lower Cone sites is testament to the flux of $\Sigma CO_2$, S, and Fe, in particular, into the overlying water column (de Ronde et al., 2011).

Shore-based analyses will focus on more detailed geochemical, isotopic, and fluid inclusion studies to decipher the conditions of alteration, the sources of elements, and the elemental exchanges that accompany fluid–rock reactions.

4. *Assess the diversity, extent, and metabolic pathways of microbial life in an extreme, metal-toxic, and acidic volcanic environment*

The overarching objectives for microbiological studies for Expedition 376 focus on determining the biomass, activity, and community structure of subsurface microbial and viral communities using an array of microbiological applications. Whole-round samples collected for microbiological studies were subsampled for shore-based analyses to explore the limits of microbial life and characterize the microbial diversity (including Bacteria, Archaea, and viruses) using cultivation-based and cultivation-independent molecular biological approaches.

Relatively few shipboard analyses were performed because most measurements require post-expedition studies in shore-based laboratories. First, detection of ATP was attempted on board to identify signs of bacterial life in the rock samples. However, detection was not successful in most cases because of denaturation of the luciferase enzyme by compounds found within the retrieved material. Second, tracers were pumped into the drill string prior and during core recovery. Systematic sampling of the cored material and drilling fluids indicated that the interiors of the whole-round samples for microbiology are suitable for shore-based analyses.

Postexpedition analyses will include an array of techniques:

- Total cell counts to quantify microbial biomass,
- DNA analysis of small-subunit ribosomal gene amplicon sequencing to address community structure,
- Metagenomics analysis to reconstruct the metabolic potential and identify entire genomes from microbial populations in the samples,
- Metatranscriptomics of total RNA to establish potential community activity (i.e., the genes that are most expressed in a given microbial environment),
- Characterization of viral diversity using polymerase chain reaction and metagenomic approaches to identify the role of viruses in the ecosystem,
- Metabolic activity measurements of microbial communities using stable isotope–labeled or radioactive isotope–labeled tracers to identify what kinds of major energy and carbon metabolisms are present, and
- Enrichment of specific groups of organisms to identify the unique physiological properties of the organisms.

# References

Baker, E.T., Embley, R.W., Walker, S.L., Resing, J.A., Lupton, J.E., Nakamura, K., de Ronde, C.E.J., and Massoth, G.J., 2008. Hydrothermal activity and volcano distribution along the Mariana arc. *Journal of Geophysical Research: Solid Earth,* 113(B8):B08S09. **https://doi.org/10.1029/2007JB005423**

Baker, E.T., Walker, S.L., Embley, R.W., and de Ronde, C.E.J., 2012. High-resolution hydrothermal mapping of Brothers Caldera, Kermadec arc. *Economic Geology,* 107(8):1583–1593. **https://doi.org/10.2113/econgeo.107.8.1583**

Barriga, F.J.A.S., Binns, R.A., Miller, D.J., and Herzig, P.M. (Eds.), 2007. *Proceedings of the Ocean Drilling Program, Scientific Results,* 193: College Station, TX (Ocean Drilling Program). **https://doi.org/10.2973/odp.proc.sr.193.2007**

Bischoff, J.L., 1991. Densities of liquids and vapors in boiling NaCl-$H_2O$ solutions: a PTVX summary from 300° to 500°C. *American Journal of Science,* 291(4):309–338. **https://doi.org/10.2475/ajs.291.4.309**

Bischoff, J.L., and Rosenbauer, R.J., 1985. An empirical equation of state for hydrothermal seawater (3.2 percent NaCl). *American Journal of Science,* 285(8):725–763. **https://doi.org/10.2475/ajs.285.8.725**

Caratori Tontini, F., Davy, B., de Ronde, C.E.J., Embley, R.W., Leybourne, M., and Tivey, M.A., 2012a. Crustal magnetization of Brothers Volcano, New Zealand, measured by autonomous underwater vehicles: geophysical expression of a submarine hydrothermal system. *Economic Geology,* 107(8):1571–1581. **https://doi.org/10.2113/econgeo.107.8.1571**

Caratori Tontini, F., de Ronde, C.E.J., Yoerger, D., Kinsey, J.C., and Tivey, M., 2012b. 3-D focused inversion of near-seafloor magnetic data with application to the Brothers Volcano hydrothermal system, southern Pacific Ocean, New Zealand. *Journal of Geophysical Research: Solid Earth,* 117(B10):B10102. **https://doi.org/10.1029/2012JB009349**

Clark, M.R., and O'Shea, S., 2001. Hydrothermal vent and seamount fauna from the southern Kermadec Ridge, New Zealand. *InterRidge News,* 10b. **https://www.interridge.org/files/interridge/IR_News_10b.pdf**

de Ronde, C.E.J., Baker, E.T., Massoth, G.J., Lupton, J.E., Wright, I.C., Sparks, R.J., Bannister, S.C., et al., 2007. Submarine hydrothermal activity along the mid-Kermadec arc, New Zealand: large-scale effects on venting. *Geochemistry, Geophysics, Geosystems,* 8(7):Q07007. **https://doi.org/10.1029/2006GC001495**

de Ronde, C.E.J., Butterfield, D.A., and Leybourne, M.I., 2012. Metallogenesis and mineralization of intraoceanic arcs I: Kermadec arc—introduction. *Economic Geology,* 107(8):1521–1525. **https://doi.org/10.2113/econgeo.107.8.1521**

de Ronde, C.E.J., Chadwick, W.W., Jr., Ditchburn, R.G., Embley, R.W., Tunnicliffe, V., Baker, E.T., Walker, S.L., Ferrini, V.L., and Merle, S.M., 2015. Molten sulfur lakes of intraoceanic arc volcanoes. *In* Rouwet, D., Christenson, B., Tassi, F., and Vandemeulebrouck, J. (Eds.), *Advances in Volcanology: Volcanic Lakes*. Nemeth, K. (Series Ed.): Berlin (Springer-Verlag), 261–288. **https://doi.org/10.1007/978-3-642-36833-2_11**

de Ronde, C.E.J., Hannington, M.D., Stoffers, P., Wright, I.C., Ditchburn, R.G., Reyes, A.G., Baker, E.T., et al., 2005. Evolution of a submarine magmatic-hydrothermal system: Brothers Volcano, southern Kermadec arc, New Zealand. *Economic Geology,* 100(6):1097–1133. **https://doi.org/10.2113/gsecongeo.100.6.1097**

de Ronde, C.E.J., Humphris, S.E., and Höfig, T.W., 2017. *Expedition 376 Scientific Prospectus: Brothers Arc Flux.* International Ocean Discovery Program. **https://doi.org/10.14379/iodp.sp.376.2017**

de Ronde, C.E.J., Massoth, G.J., Baker, E.T., and Lupton, J.E., 2003. Submarine hydrothermal venting related to volcanic arcs. *In* Simmons, S.F., and Graham, I.G. (Eds.), *Volcanic, Geothermal, and Ore-Forming Fluids: Rulers and Witnesses of Processes Within the Earth.* Society of Economic Geologists - Special Publication. 10:91–109.

de Ronde, C.E.J., Massoth, G.J., Butterfield, D.A., Christenson, B.W., Ishibashi, J., Ditchburn, R.G., Hannington, M.D., et al., 2011. Submarine hydrothermal activity and gold-rich mineralization at Brothers Volcano, Kermadec arc, New Zealand. *Mineralium Deposita,* 46(5–6):541–584. **https://doi.org/10.1007/s00126-011-0345-8**

Delteil, J., Ruellan, E., Wright, I., and Matsumoto, T., 2002. Structure and structural development of the Havre Trough (SW Pacific). *Journal of Geophysical Research: Solid Earth,* 107(B7):1–17. **https://doi.org/10.1029/2001JB000494**

Driesner, T., and Heinrich, C.A., 2007. The system $H_2O$-NaCl. Part I: correlation formulae for phase relations in temperature-pressure-composition space from 0 to 1000 °C, 0 to 5000 bar, and 0 to 1 $X_{NaCl}$. *Geochimica et Cosmochimica Acta,* 71(20):4880–4901. **https://doi.org/10.1016/j.gca.2006.01.033**

Embley, R.W., de Ronde, C.E.J., Merle, S.G., Davy, B., and Catatoni Tontini, F., 2012. Detailed morphology and structure of an active submarine arc caldera: Brothers Volcano, Kermadec arc. *Economic Geology,*107(8):1557–1570. **https://doi.org/10.2113/econgeo.107.8.1557**

Flores, G.E., Wagner, I.D., Liu, Y., and Reysenbach, A.-L., 2012. Distribution, abundance, and diversity patterns of the thermoacidophilic "deep-sea hydrothermal vent euryarchaeota 2." *Frontiers in Microbiology,* 3:47. **https://doi.org/10.3389/fmicb.2012.00047**

Freudenthal, T., and Wefer, G., 2007. Scientific drilling with the seafloor drill rig MeBo. *Scientific Drilling,* 5:63–66. **https://doi.org/10.5194/sd-5-63-2007**

Gamble, J.A., Woodhead, J.D., Wright, I.C., and Smith, I.E.M., 1996. Basalt and sediment geochemistry and magma petrogenesis in a transect from oceanic island arc to rifted continental margin arc: the Kermadec–Hikurangi margin, SW Pacific. *Journal of Petrology,* 37(6):1523–1546. **https://doi.org/10.1093/petrology/37.6.1523**

Gamble, J.A., and Wright, I.C., 1995. The southern Havre Trough geological structure and magma petrogenesis of an active backarc rift complex. *In* Taylor, B. (Ed.), *Backarc Basins: Tectonics and Magmatism:* New York (Plenum Press), 29–62. **https://doi.org/10.1007/978-1-4615-1843-3_2**

Gruen, G., Weis, P., Driesner, T., de Ronde, C.E.J., and Heinrich, C.A., 2012. Fluid-flow patterns at Brothers Volcano, southern Kermadec arc: insights from geologically constrained numerical simulations. *Economic Geology,* 107(8):1595–1611. **https://doi.org/10.2113/econgeo.107.8.1595**

Gruen, G., Weis, P., Driesner, T., Heinrich, C.A., and de Ronde, C.E.J., 2014. Hydrodynamic modeling of magmatic-hydrothermal activity at submarine arc volcanoes, with implications for ore formation. *Earth and Planetary Science Letters,* 404:307–318. **https://doi.org/10.1016/j.epsl.2014.07.041**

Haase, K.M., Stroncik, N., Garbe-Schönberg, D., and Stoffers, P., 2006. Formation of island arc dacite magmas by extreme crystal fractionation: an example from Brothers Seamount, Kermadec island arc (SW Pacific). *Journal of Volcanology and Geothermal Research,* 152(3–4):316–330. **https://doi.org/10.1016/j.jvolgeores.2005.10.010**

Haase, K.M., Worthington, T.J., Stoffers, P., Garbe-Schönberg, D., and Wright, I., 2002. Mantle dynamics, element recycling, and magma genesis beneath the Kermadec arc-Havre Trough. *Geochemistry, Geophysics, Geosystems,* 3(11):1071. **https://doi.org/10.1029/2002GC000335**

Herzig, P.M., Humphris, S.E., Miller, D.J., and Zierenberg, R.A. (Eds.), 1998. *Proceedings of the Ocean Drilling Program, Scientific Results,* 158: College Station, TX (Ocean Drilling Program). **https://doi.org/10.2973/odp.proc.sr.158.1998**

Humphris, S.E., Reysenbach, A.-L., Tivey, M., de Ronde, C.E.J., and Caratori Tontini, F., 2018. Brothers volcano, March 6-26, 2018. R/V *Thomas G. Thompson*, ROV *Jason* TN350 Cruise Report.

Lupton, J., Butterfield, D., Lilley, M., Evans, L., Nakamura, K., Chadwick, W., Jr., Resing, J., et al., 2006. Submarine venting of liquid carbon dioxide on a Mariana arc volcano. *Geochemistry, Geophysics, Geosystems,* 7(8):Q08007. **https://doi.org/10.1029/2005GC001152**

Merle, S., Embley, B., de Ronde, C. and Davy, B., 2007. New Zealand American Submarine Ring of Fire 2007 (NZASRoF'07/ROVARK), Brothers volcano, Kermadec arc, Ngatoro rift and Havre Trough, R/V *Sonne* Cruise Report. **https://www.pmel.noaa.gov/eoi/pdfs/cruisereport-kermadec07-final.pdf**

Nakamura, K., and Takai, K., 2014. Theoretical constraints of physical and chemical properties of hydrothermal fluids on variations in chemolithotrophic microbial communities in seafloor hydrothermal systems. *Progress in Earth and Planetary Science,* 1(1):5. **https://doi.org/10.1186/2197-4284-1-5**

Plank, T., Kelley, K.A., Zimmer, M.M., Hauri, E.H., and Wallace, P.J., 2013. Why do mafic arc magmas contain ~4 wt% water on average? *Earth and Planetary Science Letters,* 364:168–179. **https://doi.org/10.1016/j.epsl.2012.11.044**

Reyes, A.G., 1990. Petrology of Philippine geothermal systems and the application of alteration mineralogy to their assessment. *Journal of Volcanology and Geothermal Research,* 43(1–4):279–309. **https://doi.org/10.1016/0377-0273(90)90057-M**

Ruellan, E., Delteil, J., Wright, I., and Matsumoto, T., 2003. From rifting to active spreading in the Lau Basin—Havre Trough backarc system (SW

Pacific): locking/unlocking induced by seamount chain subduction. *Geochemistry, Geophysics, Geosystems,* 4(5):8909. **https://doi.org/10.1029/2001GC000261**

Stott, M.B., Saito, J.A., Crowe, M.A., Dunfield, P.F., Hou, S., Nakasone, E., Daughney, C.J., et al., 2008. Culture-independent characterization of a novel microbial community at a hydrothermal vent at Brothers Volcano, Kermadec arc, New Zealand. *Journal of Geophysical Research: Solid Earth,* 113(B8):B08S06. **https://doi.org/10.1029/2007JB005477**

Takai, K., and Nakamura, K., 2011. Archaeal diversity and community development in deep-sea hydrothermal vents. *Current Opinion in Microbiology,* 14(3):282–291. **https://doi.org/10.1016/j.mib.2011.04.013**

Takai, K., Nunoura, T., Horikoshi, K., Shibuya, T., Nakamura, K., Suzuki, Y., Stott, M., et al., 2009. Variability in microbial communities in black smoker chimneys at the NW caldera vent field, Brothers Volcano, Kermadec arc. *Geomicrobiology Journal,* 26(8):552–569. **https://doi.org/10.1080/01490450903304949**

Timm, C., Bassett, D., Graham, I.J., Leybourne, M.I., de Ronde, C.E.J., Woodhead, J., Layton-Matthews, D., and Watts, A.B., 2013. Louisville seamount subduction and its implication on mantle flow beneath the central Tonga-Kermadec arc. *Nature Communications,* 4:1720, **https://doi.org/10.1038/ncomms2702**

Timm, C., Davy, B., Haase, K., Hoernle, K.A., Graham, I.J., de Ronde, C.E.J., Woodhead, J., Bassett, D., Hauff, F., Mortimer, N., Seebeck, H.C., Wysoczanski, R.J., Caratori Tontini, F., and Gamble, J., 2014. Subduction of the oceanic Hikurangi Plateau and its impact on the Kermadec arc. *Nature Communications,* 5:4923. **https://doi.org/10.1038/ncomms5923**

Timm, C., de Ronde, C.E.J., Leybourne, M.I., Layton-Matthews, D., and Graham, I.J., 2012. Sources of chalcophile and siderophile elements in Kermadec arc lavas. *Economic Geology,* 107(8):1527–1538. **https://doi.org/10.2113/econgeo.107.8.1527**

Wallace, P.J., 2005. Volatiles in subduction zone magmas: concentrations and fluxes based on melt inclusion and volcanic gas data. *Journal of Volcanology and Geothermal Research*, 140(1–3):217–240. **https://doi.org/10.1016/j.jvolgeores.2004.07.023**

Wright, I.C., 1997. Morphology and evolution of the remnant Colville and active Kermadec arc ridges south of 33°30′S. *Marine Geophysical Research,* 19(2):177–193. **https://doi.org/10.1023/A:1004266932113**

Wright, I.C., and Gamble, J.A., 1999. Southern Kermadec submarine caldera arc volcanoes (SW Pacific): caldera formation by effusive and pyroclastic eruption. *Marine Geology,* 161(2–4):207–227. **https://doi.org/10.1016/S0025-3227(99)00040-7**

Wright, I.C., Parson, L.M., and Gamble, J.A., 1996. Evolution and interaction of migrating cross-arc volcanism and backarc rifting: an example from the southern Havre Trough (35°20′–37°S). *Journal of Geophysical Research: Solid Earth,* 101(B10):22071–22086. **https://doi.org/10.1029/96JB01761**